OPTICAL CHARACTERIZATION FOR SEMI-INSULATING GALLIUM ARSENIDE

by

Yu Zhang

B.Sc., Zhejiang University, Hangzhou, China. 1982

M.Sc., Zhejiang University, Hangzhou, China. 1986

THESIS SUBMITTED IN PARTIAL FULFILLMENT OF

THE REQUIREMENTS FOR THE DEGREE OF

DOCTOR OF PHILOSOPHY

in the Department

of

Physics

SIMON FRASER UNIVERSITY

December 1990

APPROVAL

Name: Yu Zhang

Degree: Ph.D. Physics

Title of Thesis: Optical Characterization for Semi-insulating Gallium Arsenide

Examining Committee:

Chairman: Dr. E.D. Crozier

Dr. M.L.W. Thewalt
Senior Supervisor

Dr. G. Kirczenow

Dr. S.R. Morrison

Dr. A.E. Curzon

Dr. J.S. Blakemore
External Examiner
Western Washington University

Date Approved: December 18, 1990

PARTIAL COPYRIGHT LICENSE

I hereby grant to Simon Fraser University the right to lend my thesis, project or extended essay (the title of which is shown below) to users of the Simon Fraser University Library, and to make partial or single copies only for such users or in response to a request from the library of any other university, or other educational institution, on its own behalf or for one of its users. I further agree that permission for multiple copying of this work for scholarly purposes may be granted by me or the Dean of Graduate Studies. It is understood that copying or publication of this work for financial gain shall not be allowed without my written permission.

Title of Thesis/Project/Extended Essay

Optical Characterization for Semi-insulating Gallium Arsenide

Author: _____ _____ _____
(Signature)

Yu Zhang
(Name)

Dec 20 '90
(Date)

ABSTRACT

A series of optical techniques have been used for nondestructive characterization of semi-insulating GaAs. These techniques include regular photoluminescence, photoluminescence excitation spectroscopy, time-resolved photoluminescence, selective donor-acceptor pair luminescence, electronic Raman scattering, and local vibrational mode absorption for the identification and concentration determination of acceptors. Polariton photoluminescence was employed to assess the surface treatment. For shallow donors, resonant photoluminescence can determine the concentration of the total shallow donors relative to the shallow acceptors, while magneto-photoluminescence can determine the chemical identity and relative concentration of shallow donors. For the important deep donor EL2, absorption and bleaching experiments determine the neutral EL2 concentration. The validity of these measurements was tested by comparing the predicted electron density to the measured Hall carrier density. The Fermi level and hence the carrier concentration was deduced using the three level model of semi-insulating GaAs.

ACKNOWLEDGEMENTS

I would like to thank my supervisor Dr. Mike Thewalt for his guidance throughout this project. Without his experimental skills, these experiments could not have been conducted.

I would like to thank Dr. Maria Masciaszek and Mr. R.P. Bult from Johnson Matthey Electronics Ltd. (Cominco) for providing me with thousands of samples used in this work.

The generous financial support of the Natural Science and Engineering Research Council, Simon Fraser University and Dr. M. Thewalt are also gratefully acknowledged.

Thanks to my wife Wenjia for everything.

LIST OF ABBREVIATIONS

BE	bound exciton
CB	conduction band
CFD	constant fraction discriminator
CW	continuous wave
DAP	donor-acceptor pair
EL2	main deep-donor level in undoped GaAs
ERS	electronic Raman scattering
FE	free exciton
LEC	liquid-encapsulated Czochralski
LO	longitudinal optical (phonon)
LPB	lower polariton branch
MBE	molecular beam epitaxy
MOCVD	metalorganic chemical vapor deposition
PHA	pulse-height analyzer
PL	photoluminescence
PLE	photoluminescence excitation
PM	photomultiplier
SI	semi-insulating
SPL	selective pair luminescence
TAC	time-to-amplitude converter
TO	transverse optical (phonon)
UPB	upper polariton branch
VB	valence band

CONTENTS

LIST OF FIGURES

LIST OF TABLES

CHAPTER 1: INTRODUCTION

1.1. Semi-insulating GaAs

Over the past ten years the emergence of high performance GaAs integrated circuit technologies has accelerated the demand for high-quality, large-diameter semi-insulating GaAs substrates. The new device technologies, including digital integrated circuits, monolithic microwave integrated circuits, and charge coupled devices, have largely adopted direct ion implantation as the key fabrication technique for the formation of doped layers. Ion implantation lends itself to good uniformity and reproducibility, high yield and low cost; however, these techniques also place stringent demands on the quality of the semi-insulating GaAs substrates.

Semi-insulating GaAs is generally classified by its electrical resistivity at room temperature, with values ranging from 10^6 to 10^9ohm-cm. It belongs to the semiconductor family which has the electrical resistivity in the range of 10^{-2} to 10^9ohm-cm.

If the semiconductor crystal is so pure that impurities contribute negligibly to the resistivity, one speaks of an "intrinsic semiconductor". In the intrinsic case, conduction band electrons can only come from formerly occupied valence band levels, leaving holes behind them. The conduction band is vacant at absolute zero and is separated by an energy gap E_g from the filled valence band. The band gap is the difference in energy between the lowest point of the

conduction band and the highest point of the valence band. The lowest point in the conduction band is called the conduction band edge; the highest point in the valence band is called the valence band edge. At a given temperature T, some electrons will be thermally excited into the conduction band. The number, n, of these electrons is given by

$$n = \int_{E_c}^{\infty} g_c(E)\, dE/[(\exp(E-E_F)/kT) + 1\ ] \qquad (1.1)$$

where k is the Boltzmann constant, and T the temperature. $g_c(E)$ is the number of energy levels per unit energy interval in the conduction band (the density of states), E_c is the band edge energy of the conduction band. E_F is the Fermi level of the material, which lies in the middle of the energy gap for the pure GaAs.

In practice, absolutely pure crystals do not exist. The presence of defects and impurities in the crystal lattice of a semiconductor, results in the presence of donors and acceptors in the forbidden band, and affects the conductivity very significantly.

Donors are atoms that, when present in the crystal lattice, have more valence electrons than required to complete the bonds with neighboring atoms. The presence of these atoms affects the distribution of energy states in the immediate vicinity, and extra levels are formed in the forbidden band, close to the conduction band. These donor levels can give up their electrons to the conduction band. As the energy difference is small, at room temperature some donor atoms are usually ionized. The positive charge due to the valence level is bound to the atom site. The semiconductor is said to be n-type if the

number of the conduction electrons is greater than the number of mobile holes.

Acceptors are atoms that have fewer valence electrons than required to complete the bonds with neighboring atoms, and they therefore accept electrons from any available source to complete the bonds. These extra electrons are almost as tightly bound to the atoms as the valence electrons and the presence of acceptors results in energy levels just above the valence band. The electrons in the valence band only need a small increment of energy to occupy the acceptor levels and provide the source of electrons for the acceptor atom. At room temperature, mobile holes are then left in the valence band but the electrons are bound to the acceptor atom, which is ionized by the electron capture. When the number of the acceptor atoms exceeds the number of the donor atoms, mobile holes predominate and the semiconductor is known as p-type.

The effect of the acceptors and donors is to move the Fermi-level nearer to the conduction band in n-type semiconductors and nearer to the valence band in p-type as the distribution of available energy levels has changed. The conductivity of an extrinsic semiconductor will depend on the type and amount of acceptors and donors present, and this may be controlled by adding impurities of a particular sort to achieve the desired type of conductivity. Through careful compensation, it is possible to produce a semiconductor with properties similar to an intrinsic semiconductor.

In practice, the insulating property of semi-insulating GaAs is due to the compensation of residual shallow dopant acceptors and donors

by deep levels associated with various defects among which the most important is the so-called EL2 defect. With this compensation, it is possible to produce GaAs with properties similar to an intrinsic GaAs, with the Fermi level near the middle of the band-gap. The choice of quantitative value for the definition of "shallow" and "deep" acceptors (or donors) is arbitrary because there is at present no universally accepted criterion [80J] [83N]. In GaAs, the shallow acceptors, like C, Zn, Cd, Si, and Mg, have an ionization energy of about 30meV; and we thus regard acceptors as deep acceptors for an energy more than 40meV, like Mn, Cu, Cr, and Ga_{As} antisite defect. Most donors in GaAs are very shallow, such as S, Sn, Si, and Ge, which have an ionization energy less than 10meV. Thus, the intrinsic defect EL2, with an ionization energy of 1/2 the gap, is clearly a deep donor.

GaAs single crystals have traditionally been grown by the so-called Bridgman method. However, this did not result in high-resistivity GaAs. Contamination by Si (10^{16}-$10^{17}cm^{-3}$) impurities from quartz boats was responsible for this result. Semi-insulating material was obtained by compensation of the residual impurities with deep-impurities, usually Cr. However, excessive compensation causes major problems. A conductive surface layers (called "conversion layer") sometimes forms after high-temperature heat treatment. This conversion layer is due to the out-diffusion of Cr and redistribution of the residual impurities during thermal processing [82K].

Most of these problem have been solved partially by the liquid-encapsulated Czochralski (LEC) growth technique [82H]. In this method the GaAs melt is contained in a boron nitride crucible.

Dissociation of the volatile As from the GaAs melt is avoided by encapsulating the melt in an inert molten layer of boric oxide and pressurizing the chamber with a nonreactive gas, to counterbalance the As dissociation pressure. In situ compound synthesis can be carried out from elemental Ga and As, since boric oxide melts at low temperature (450°C).

As a result of the boron nitride crucible, in situ synthesis, and the gettering effect of boric oxide encapsulation, GaAs with low nonintentional background doping level ($<10^{15}cm^{-3}$) can be grown. Semi-insulating materials (~ 10^{8} Ω cm) can be obtained by this method without using Cr as a compensating dopant.

The compensation in LEC GaAs is primarily achieved by the deep trap EL2. The amount of EL2 can be controlled by the melt stoichiometry. LEC GaAs is pure enough to reveal the contribution of native defects in the crystal. The LEC method has produced large (10 cm diameter), thermally stable high resistivity crystals.

Sometimes, electronic devices and integrated circuits do not work as expected once they are fabricated. A principal reason is the existence of defects and impurities in the bulk materials or at the surface and interfaces, which originate from the material itself or are produced during various steps of its technological processing. In fact, defects and impurities play a major role in the electronic properties of semi-conductor materials because they interact with free carriers as scattering centers, traps and recombination centers, and their effect is non-negligible even when their concentration is very small compared to the free-carrier concentration. Their effect will

become more and more important as the scale of devices decreases. For these reasons the identification and characterization of defects and impurities in semi-insulating GaAs is very important and remains an active field of research [82B] [88B] [89B].

1.2. Free Excitons

Reflectance and absorption spectra of semiconductors often show structure for photon energies just below the energy gap, where we might expect the crystal to be transparent. This structure is caused by the absorption of a photon with the creation of an "exciton". An electron and a hole may be bound together by their attractive electrostatic interaction, just as an electron is bound to a proton. The bound electron-hole pair is called an exciton. It can move through the crystal transporting excitation energy, but it is electrically neutral.

There are two forms of excitons, one involving a very localized state, the Frenkel exciton and the other, by contrast a much more extended state, the Wannier-Mott exciton. The Frenkel exciton has a radius comparable with the interatomic separation and is typically exemplified in strongly ionic crystals with low mobility and dielectric constant, such as alkali halides. According to quantum mechanical principles, one would expect the binding energy of the exciton to be large, due to the high degree of localization. The Wannier-Mott exciton is found in materials having a large degree of covalent bonding, high mobility and large dielectric constant, such as GaAs, which is the subject of this thesis.

The Mott-Wannier exciton is a weakly bound exciton, with an average electron-hole distance large in comparison with a lattice constant. Consider an electron in the conduction band and a hole in the valence band. The electron and hole attract each other by the Coulomb potential

$$U(r) = -e^2/\varepsilon r, \tag{1.2}$$

where r is the distance between the particles and ε is the appropriate dielectric constant. There will be bound states of the exciton system having total energies lower than the band gap energy.

The exciton is very similar to the hydrogen atom, if the energy surfaces for the electron and hole are spherical and nondegenerate. The excitons are free to move through the crystal, leading to a series of excitonic levels. The energy levels referred to the crystal ground state are given by a modified Rydberg equation

$$E_x = E_g - \mu e^4/(2\hbar^2\varepsilon^2 n^2) + \hbar^2K^2/(2M) \tag{1.3}$$

Here n is the principal quantum number, $\hbar K$ is the momentum of the exciton center of mass, M is the total mass of an exciton, and μ is the reduced mass:

$$M = m_e + m_h \tag{1.4a}$$

$$1/\mu = 1/m_e + 1/m_h , \tag{1.4b}$$

formed from the effective masses m_e, m_h of the electron and hole.

Pursuing the analogy with the H atom, we see that, disregarding the normalization factor, the wave function of the n=1 exciton is

$$\psi(\mathbf{R},r) = \exp(i\mathbf{k}\cdot\mathbf{R} - r/a_x) , \tag{1.5}$$

where **R** is the center of mass coordinate, and the most probable value of r is a_x, the exciton Bohr radius, given by

$$a_x = \hbar^2\varepsilon/(\mu e^2). \qquad (1.6)$$

The binding energy of the n=1 free exciton, relative to a free electron-hole pair at the band-edge, called the exciton Rydberg (R_x), is

$$R_x = \mu e^4/(2\hbar^2\varepsilon^2) = e^2/(2\varepsilon a_x) = \hbar^2/(2\mu a_x^2) \qquad (1.7)$$

which provides a convenient way of estimating a_x from E_x. In GaAs, for which $\varepsilon = 12.5$ and $\mu = 0.058\ m_o$ where m_o is the free electron mass, one obtains R_x = 5meV and a_x = 110Å. Hence, all of the exciton states except n=1 are within 1.25meV of the band gap energy and are not easily distinguished from band gap emission. At low temperature the n=1 exciton line should dominate the emission spectrum and will occupy most of our attention.

When the electron recombines with the hole, the FE annihilates, giving up its energy to create a slightly below band-gap photon, which can be detected outside the crystal. The momentum selection rule allows only those excitons with nearly zero kinetic energy to decay into photons. However, this condition does not prevent excitons from possessing kinetic energy. Exciton emission at other than zero kinetic energy can occur through phonon participation, because phonons provide

additional means of satisfying the momentum selection rule.

Phonon energies and momenta are denoted as $\hbar\omega_{ph}$ and $\mathbf{q}_{ph}$. When it is necessary to distinguish between acoustic and optical phonons, the subscript "ph" will be replaced by "A" or "O". If even further distinction is required as to transverse or longitudinal modes, the subscripts will read TA, TO, LA, or LO. Let $\mathbf{k}$ be the photon wave vector and $\hbar\omega$ be the photon energy. Let us consider two paths for exciton annihilation. Photon emission can occur together with

(1). Zero-phonon emission

$$\mathbf{K} = \mathbf{k} = 0 \tag{1.8a}$$

$$\hbar\omega = E_x \tag{1.8b}$$

(2). One-phonon emission

$$\mathbf{K} = \mathbf{k} + \mathbf{q}_{ph} \tag{1.9a}$$

$$\hbar\omega = E_x - \hbar\omega_{ph} \tag{1.9b}$$

We consider the longitudinal optical (LO) phonon replication lines. The optical phonon energies are usually nearly independent of momentum, particularly for small $\mathbf{q}$. Thus $\hbar\omega_{LO}$ is the same for all $\mathbf{q}_{LO}$ [77S]. It follows that the phonon replica is not significantly broadened by phonon dispersion and occurs at a photon energy of

$$\hbar\omega = E_x - \hbar\omega_{LO} \tag{1.10}$$

While $\hbar\omega_{LO}$ might be assumed independent of q_{LO}, the total exciton energy E_X contains the kinetic energy of exciton motion

$$E_X(K) = E_g - R_X/n^2 + \hbar^2K^2/(2M) \qquad (1.11)$$

and thus depends on the value of **K**.

In practice, however, the line shape for a free exciton is always broad. The line shape has been calculated in several approximations by Toyozawa [58T]. He assumes that the line width is essentially determined by the lifetime of **K**=0 excitons before they are scattered to other momentum states **K**≠0 by phonons. It is well known that an eigenstate can be perfectly sharp only if its lifetime is infinite. If its lifetime is finite, then, according to the uncertainty principle $\Delta E \Delta\tau > \hbar$, some uncertainty in its energy is necessary. In this way, the width of the exciton line is determined in part by all of the processes which limit the time that the exciton spends in the **K**=0 state, including phonon scattering.

Toyozawa obtained analytical expressions for the line shapes in the two limiting cases of weak and strong phonon coupling. The line shape for weak coupling is a Lorentzian curve, wheres for strong exciton-phonon coupling, a Gaussian curve is obtained. In the III-V compounds, weak exciton-phonon coupling should prevail. Other effects may obscure the expected line shape. Crystal imperfections, impurities, and strains can cause inhomogeneous broadening of the exciton line. If this type of broadening prevails, then the observed line will probably approximate a Gaussian no matter what line shape is

anticipated for a perfect crystal.

Dissociation of a free exciton into a free electron and a free hole is another process capable of shortening the lifetime of an exciton, and therefore broadening the line shape. Dissociation can occur when the kinetic energy of the exciton exceeds its binding energy. Toyozawa [58T] [62T] calculated the lifetime due to dissociation involving absorption or emission of a phonon assuming the exciton energy is distributed according to the Maxwell-Boltzmann law. This process is of particular interest because its reverse leads to the formation of excitons from free electrons and holes which might be generated in a photoluminescence experiment by the excitation light. He found, for temperatures such that kT is less than the exciton binding energy, that the formation of n=1 excitons is more probable than band to band radiative recombination of the electron and hole.

1.3. Bound Excitons

So far we have considered the excitons only in perfect crystals. Real crystals contain impurities and defects, and even in GaAs, which, because of its technical importance is available with an impurity content of the order of $10^{15}cm^{-3}$ or less, these play a crucial role. In particular, as we shall see, excitons bound to impurities tend to dominate the optical emission spectra at low temperatures.

The total energy of an exciton can be decreased by the presence of a point defect or an impurity such as a donor or an acceptor. If the total energy of the system is reduced when the exciton is in the vicinity of an impurity, then it is energetically favorable for the free exciton to remain near the defect. The exciton becomes bound to the impurity to form a bound exciton at low enough temperature. Hopfield [64H] established that the bound exciton stability criterion depends on the electron-hole effective mass ratio ($\sigma=m_e/m_h$). He concluded that excitons bound to neutral impurities are stable for all possible mass ratios, while excitons bound to ionized impurities are stable only for restricted values of σ. In GaAs, where m_e is much smaller than m_h ($\sigma=m_e/m_h=0.15$), an exciton bound to an ionized donor is stable while an exciton bound to an ionized acceptor is not. The intuitive argument used to support this result is that when the electron and hole masses are very different, the heavy particle will move close to the ionized impurity, the lighter particle will be at a greater distance, from which the ionized center and the more massive particle will look like a neutral impurity [69L]. The lighter particle

will then not bind to the apparent neutral impurity.

The differences in exciton localization energy on different donors or acceptors are due to the impurity-specific central cell potential, which must be added to the Coulomb interaction for donor and acceptor bound exciton. The central cell corrections often leads to linear dependence of bound exciton binding energy E_{BE} on impurity binding energy E_i [60H]

$$E_{BE} = a + bE_i \ , \tag{1.12}$$

where a and b are constant for a given material. Equation (1.12) is often called Haynes' rule.

Reynolds [82R] and Dean [73D] using an idea first suggested by Hopfield, have attempted to explain the general trend by using a first order perturbation theory. These authors introduced a central cell potential V_c and assumed a linear dependence of both E_{EX} and E_i on V_c of the form

$$E_i = (E_i)_{EM} + V_c\rho \tag{1.13}$$

$$E_{BE} = (E_{BE})_{EM} + V_c\rho' \tag{1.14}$$

where the subscript EM refers to the effective mass binding energy with zero central cell correction. ρ denotes the electronic charge in the central region of the neutral donor and ρ' denotes the modified electronic charge in the same region due to the presence of an exciton.

These equations can be combined in the form

$$E_{BE} = [(E_{BE})_{EM} - (E_i)_{EM} (\rho'/\rho)] + (\rho'/\rho) E_i \qquad (1.15)$$

and now the constants a and b in equation (1.12) may be identified as

$$a = [(E_{BE})_{EM} - (E_I)_{EM} (\rho'/\rho)], \text{ and } b = \rho'/\rho \qquad (1.16)$$

In the case of GaAs, Sharma and Rodriguez [67S] predicted a binding energy for an exciton X trapped on an ionized donor, D^+ of $E(D^+,X) = 1.06\ E_D$, where E_D is the binding energy of the isolated donor. The binding energy for excitons bound to neutral impurities is usually expressed in terms of the dissociation D^0 (or A^0), i.e., the energy required to separate the complex into a neutral impurity and a free exciton. For excitons bound to neutral donors (D^0,X), Sharma and Rodriguez calculate a dissociation energy of $D^0=0.13E_D$, giving a binding energy of $E(D^0,X)=E_X+0.13E_D$. Here E_X is the binding energy of the free exciton. Sharma and Rodriguez have not considered the exciton-neutral acceptor complex (A^0,X). Hopfield [64H] gives $E(A^0,X)=E_X+0.07E_A$ for this case. Collecting the results, Bogardus and Bebb estimated the photon emission energy $h\upsilon$ of radiative annihilation of the exciton complexes (D^0,X), (D^+,X), and (A^0,X) to be [68B]

$$h\upsilon(D^0,X) = E_g - E_X - 0.13E_D , \qquad (1.17a)$$

$$h\upsilon(D^+,X) = E_g - E_D - 0.06E_D , \qquad (1.17b)$$

$$h\upsilon(A^0,X) = E_g - E_X - 0.07E_A , \qquad (1.17c)$$

From effective mass arguments based on the hydrogenic model, we have E_X=4.4meV, $E_D=(1+\sigma)E_X$=5.2meV, and $E_A=E_D/\sigma$=34meV, where σ=0.15 for GaAs. For Si in GaAs, E_D=6.8 meV and E_A=29.7meV. Using these values together with E_X=4.4meV, Eqs.(1.17a)-(1.17c) give 1514.5, 1513.3, and 1512.5meV, respectively, for the emission energies.

The bound exciton lines are distinguished from a free exciton by their sharp-line optical transitions in photoluminescence. The sharp spectral lines of bound excitons can be very intense. The line intensities, in general, depend on the concentrations of donors and/or acceptors present in the samples [60H], and the presence of the other traps which compete in capturing electrons, holes or excitons.

In general, exciton states are observed only in relatively pure GaAs crystals. This occurs for a number of reasons. First, the electron-hole interaction is strongly shielded by the presence of other free carriers in the system. Casella [63C] has indicated, in fact, that for free carrier concentrations greater than $5\times10^{-2}\ a_x^{-3}$ no bound exciton states can exist. For a_x= 110 Å, as found in GaAs, the upper carrier concentration limit is thus $2\times10^{16}cm^{-3}$. Exciton effects will therefore be important in semi-insulating GaAs with lower impurity concentrations of the order of $10^{15}cm^{-3}$.

1.4. Polaritons

Polaritons result from the coupling of light to polarization modes in a medium, such as phonons and excitons. In this thesis, we are only interested in excitonic polaritons which determine the intrinsic optical properties of many direct gap semiconductors. As a result the term polariton will be understood to mean exciton-polaritons unless otherwise stated.

The exciton has a polarization $\mathbf{P}\exp(i\mathbf{k}\cdot\mathbf{R})$ associated with it, and like an optic phonon, can be longitudinal ($\mathbf{P}\parallel\mathbf{K}$) or transverse ($\mathbf{P}\perp\mathbf{K}$). Only the transverse exciton can interact with an electromagnetic field. This (dipolar) interaction splits the exciton into longitudinal and transverse branches. Fig. 1.1 is a schematic E(K) diagram for the transverse exciton, and for the photon [57P][82Ra]. As in the analogous case of the optical phonon [51H] [65H], the photon and the transverse exciton mix in the crossover region, losing their identity in a combined particle called excitonic-polariton or polariton [58H] (the dashed "light lines"). The coupling opens up a gap at crossing point resulting in a two branch polariton dispersion curve given by

$$(\hbar ck/E)^2 = \varepsilon_0 + 2\varepsilon_0 E_{LT} E/[E_0(k)^2 - E^2], \qquad (1.18)$$

where ε_0 is the dielectric constant in the absence of the polaritons, E_{LT} is the splitting between the longitudinal uncoupled free exciton and the coupled transverse polaritons and thus is a measure of the coupling strength, E is the polariton energy and $E_0(k)$ is the energy of

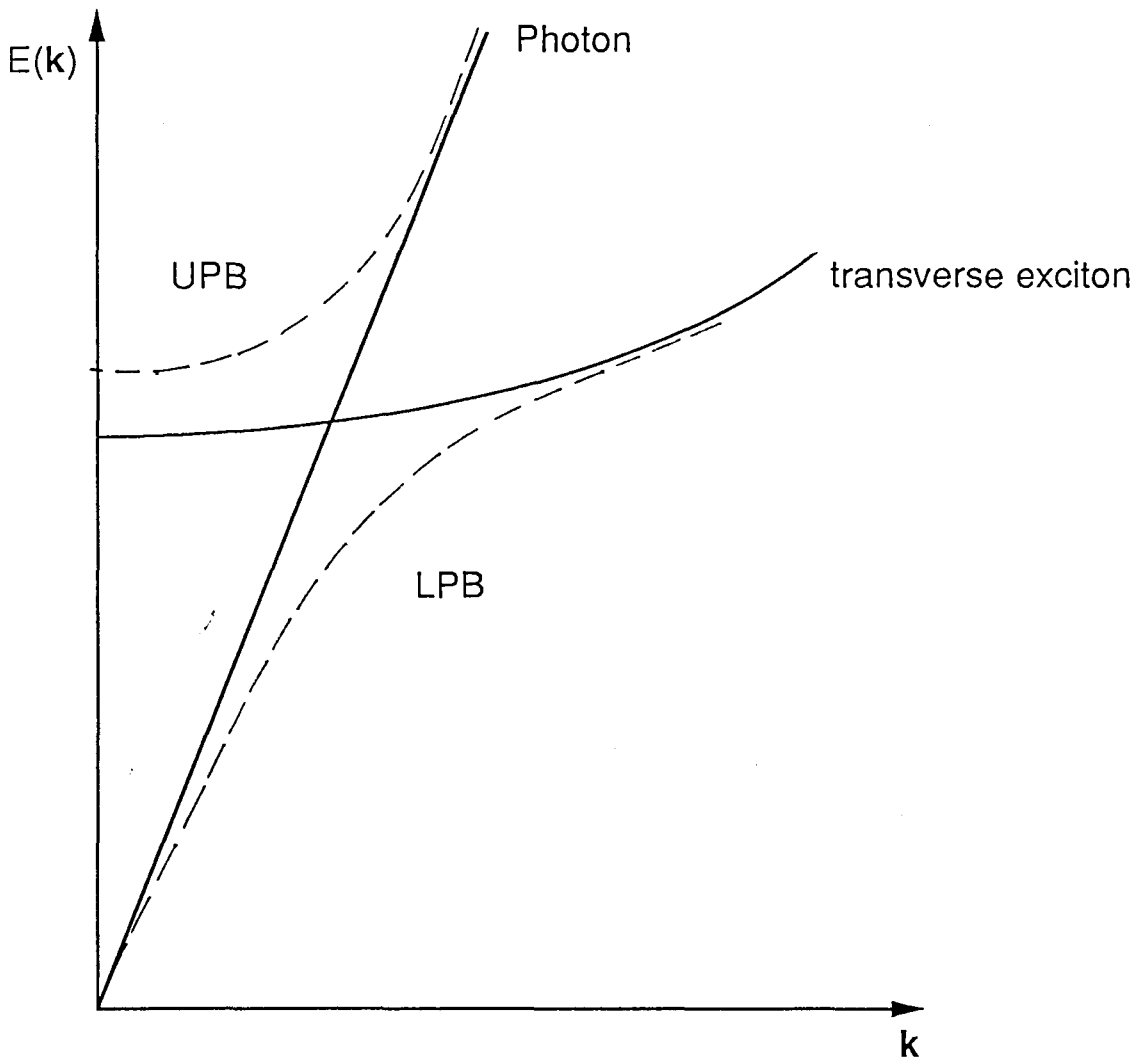

Fig. 1.1. Dispersion curves for the photon, transverse exciton, and polariton (dashed curves). The upper (UPB) and lower (LPB) polariton branches are labelled.

the uncoupled free exciton of wavevector k which is equal to the transverse exciton energy E_T plus the kinetic energy term. In the near resonance region ($E_0(k)-E<<E$), the dispersion relation can be approximated by

$$(\hbar ck/E)^2 = \varepsilon_0 + \varepsilon_0 E_{LT}/[E(k)_0 - E]. \qquad (1.19)$$

The polariton dispersion curve appropriate for GaAs [86S] shows that, on the lower branch (LPB), at large wave vectors, the polaritons are predominantly exciton-like, whereas at small wave vectors they are photon-like; on the upper branch (UPB) the polaritons start out exciton-like but rapidly become photon-like with increasing wave vector.

The existence of two polariton branches means that for a given frequency there can exist as many as two propagating waves inside the medium with the same polarization but with different wave vectors. The existence of this additional transmitted wave means that the Maxwell's equations when applied to the fields at the surface of the medium are insufficient for determining uniquely the transmitted and reflected wave amplitudes. Under such circumstances an additional boundary condition (known as ABC) is needed. Extensive theoretical and experimental investigation of this condition have already been documented in the literature [79Y]. However, the situation is far from being clear. Experimental results obtained by different techniques on the same sample appear to require different additional boundary conditions [85A].

The experimentally observed polariton spectrum is usually a

doublet structure, which has been interpreted in many ways [73S] [79A] [77W]. Recently it has been suggested that in GaAs polariton impurity scattering is the dominant scattering mechanism at low temperatures, and experimentally shown that elastic neutral donor scattering has a marked effect on the polariton luminescence shape, and is consequently the scattering mechanism responsible for the absorption [85K] [85B].

For GaAs, Steiner and Thewalt [86S] [86Sb] have constructed a model of polariton luminescence using a time-dependent Boltzmann equation and considering only elastic neutral donor scattering. Any mechanism which affects the transport of a polariton to the sample surface, the probability of transmission at the surface, the distribution of polaritons in the crystal, or the polariton energy distribution can influence the observed polariton luminescence. Consequently, one can expect great variations in the observed emission with different samples, experimental conditions or surface preparation.

1.5. Non-excitonic Transitions

Besides the exciton emissions, non-excitonic luminescence lines, which are either neutral donor to neutral acceptor pair (DAP) recombinations or free carrier to neutral impurity transitions, are also observable in semiconductors. Donor-acceptor pair complexes differ in certain obvious respect from exciton complexes bound to point defects, but they also retain many similarities. Like the exciton-neutral impurity complex, the donor-acceptor pair consists of four point charges. It differs in that two of them are immobile, the donor ion D^+ and the acceptor ion A^-.

Because the separation of the donor and acceptor ions is fixed by their positions in the crystal lattice, a constraint is introduced which eliminates positions in the crystal lattice $R=|R_D-R_A|$ as a degree of freedom for a given pair. Thereby, in the computation of the binding energy, R is not a conjugate variable (or operator) of the system but is reduced to a parameter which can be specified in the classical sense (neglecting small oscillations in R due to lattice vibrations). Accordingly, the binding energy of the complex is determined by minimizing the expectation value of the energy for a fixed R. Two cases are distinguished: (1). distant donor-acceptor pairs when the separation R between the donor and acceptor ions is much greater than the Bohr radii of either the neutral donor or neutral acceptor and (2). close pairs, where R is comparable to or smaller than the Bohr radii of either the donor or acceptor.

Consider a donor which has been compensated by an acceptor so that

both are charged D^+ and A^-. Take this as the zero of energy. Now the energy required to form the complex is the energy E_g required to excite an electron to the conduction band leaving behind a hole in the valence band, reduced by the energy gained by the electron on D^+ in the presence of of A^- at a distance R away, $-E_D + e^2/\varepsilon R$, and then binding the hole on A^- in the presence of D^o, $-E_A$. In other words, the binding energy of the donor E_D is reduced by the repulsive potential $-e^2/\varepsilon R$ arising from the ionized acceptor at the distance R, but the subsequent process of placing a hole on the acceptors is not greatly altered by the presence of the distant neutral donor and hence involves only the acceptor binding energy E_A. A small energy contribution due to the polarizabilities of the neutral donor and acceptor can be included as a correction term J(R), hence

$$\hbar\omega(R) = E_g - (E_A + E_D) + e^2/\varepsilon R + J(R). \qquad (1.20)$$

where J(R) is negligible for large separation. Other energy cycles can also be followed to arrive at Eq. (1.20).

For substitutional impurities, the donors and acceptors in the pairs must be on lattice sites, so the separation R takes discrete values, with a distribution depending on the statistical arrangement of donors and acceptors. For the relative small R corresponding to say 10 to 50 lattice spacings, the change in the energy $e^2/\varepsilon R$ between lattice shells can be resolved and the spectrum $\hbar\omega(R)$ appears as a discrete set of emission lines corresponding to the allowed values of R. As $e^2/\varepsilon R \rightarrow 0$ and the emission lines from neighboring lattice shells become

increasingly close together, eventually merging to form a broad band of emission energies with the low energy limit occurring for $\hbar\omega(\infty) = E_g - E_D - E_A$ as R approach infinity. The intensity of the various portions of the spectrum $\hbar\omega(R)$ are determined by the overlap of the donor and acceptor wave functions and the number of interacting pairs. Generally, the number of acceptors contained in a shell of thickness dR at a distance R from a donor at say R = 0 increases as R^2. However, for smaller values of R, the discreteness of the lattice causes violent fluctuation in the intensities of discrete emission lines. The intensity fluctuations can be used as an aid to identifying the spectra since they are predictable from the geometry just by counting the available lattice sites corresponding to a given R. Consequently, a series of sharp luminescence lines corresponding to individual pairs can sometimes be observed at low temperature. The merging of the discrete lines to form the broadband emission as $R \rightarrow \infty$ has been also observed in some semiconductors.

Hopfield [63H] first analyzed the recombination due to donor acceptor pairs in GaP in terms of Eq. (1.20). Sharp line spectra attributed to donor-acceptor pair recombination have also been identified in BP [66R] and AlSb [68L], both indirect-gap semiconductors similar to GaP. But they have not yet been seen in any direct-gap III-V compounds, such as GaAs.

Gershenzon [66G] proposed that sharp pair lines will not be observed for hydrogenic centers in GaAs because the sum of the (shallow) donor and (shallow) acceptor binding energies in GaAs are typically rather small. The pair lines would, consequently, all be

above the band gap because $e^2/\varepsilon R > E_D + E_A$ for the corresponding values of R. Only the unresolved broadband portion of the pair spectra is expected to be observable.

In the absence of sharp lines, more indirect evidence of donor-acceptor pair recombination must be pursued. Gershenzon [66G] first suggested that the 1490meV line observed in undoped GaAs in the low temperature range might be a donor-acceptor pair band associated with carbon acceptor (D^0,C). This suggestion led Leite and DiGiovanni [67L] to conduct a thorough investigation of the 1490meV line in undoped n-type melt-grown GaAs. They observed a series of characteristics of the 1490meV line which they considered to be evidence for donor-acceptor emission [67L].

Besides donor-acceptor pair luminescence, free-to-bound transitions, such as free-electron to neutral acceptor (e,A^0) or free-hole to neutral donor (h,D^0), are also observed in the near gap photoluminescence spectrum of various semiconductors. The energy of such photons would correspond simply to the difference between the band gap energy and the ionization energy of the neutral impurity, plus the initial kinetic energy of the free particle. For GaAs, the 1493meV luminescence peak observed at 2K is attributed to the free electron to neutral carbon acceptor (e,C^0) transition, while the 1490meV luminescence peak corresponds to the free electron to zinc acceptor (e,Zn^0) transition, which overlaps with donor-acceptor pair band of carbon(D^0,C) [75A].

CHAPTER 2: EXPERIMENTAL APPARATUS

2.1. Introduction

Optical techniques have proved themselves to be very useful for the assessment of semiconductor materials. Impurities and native defects which are present in concentrations below $10^{14}cm^{-3}$ can be detected without the destruction of the sample. Furthermore, optical techniques are fast, allowing the routine testing of a large number of samples [89S] [89M] [90S] [90Sa].

Generally speaking, the experimental apparatus for optical characterization of semiconductors consists of the following: (a) light sources, which may include ordinary lasers, tunable lasers, mode-locked lasers, monochromaters and so on; (b) samples and their environments, e.g. temperature, magnetic field, stress etc.; (c) data acquisition systems, which are usually made up of spectrometers, detectors, and computers (hardware and software). This chapter is concerned with these techniques and instrumentation used in the observation and measurement of semi-insulating GaAs.

2.2. Spectroscopic Light Sources

In this work, an Argon ion (Ar^+) laser (Spectra-Physics Model 171) was used as the above band gap excitation source for the ordinary photoluminescence work, or used as a pump for a dye laser (Spectra-Physics Model 375) or Ti:Sapphire laser (Spectra-Physics Model 3900) for resonant excitation of the near-gap photoluminescence. The discharge of a CW Argon laser exhibits gain for more than fifteen different transitions, among which the two strongest emission lines are at 488nm and 514.5nm. In order to achieve single-line oscillation in laser media which exhibit gain for several transitions, wave-length-selecting elements outside or inside the laser resonator are usually employed.

The gain medium of a dye laser is a liquid solution of an organic dye which absorbs pump laser light focused on it by the input mirror (see Figure 2.1a) and emits light at longer wavelengths through fluorescence. This emitted light passes through the dye stream many times as it is reflected back and forth between the mirrors which form the optical cavity of the dye laser. As light passes through the dye stream, dye molecules previously excited by the pump light are stimulated to emit light at the fluorescence wavelengths, providing laser action. A tuning wedge tunes the resonant cavity to any point within the broad fluorescence bandwidth and a fine tuning etalon provides narrowed output linewidth and finer control of output wavelength.

Although several dye solutions are available, we mainly use 90 ml

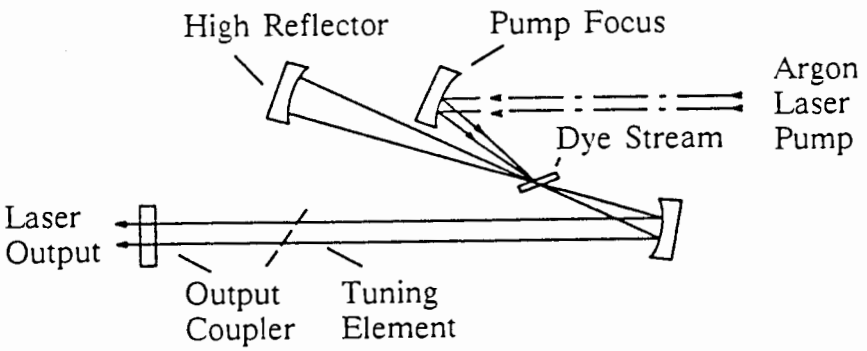

(a)

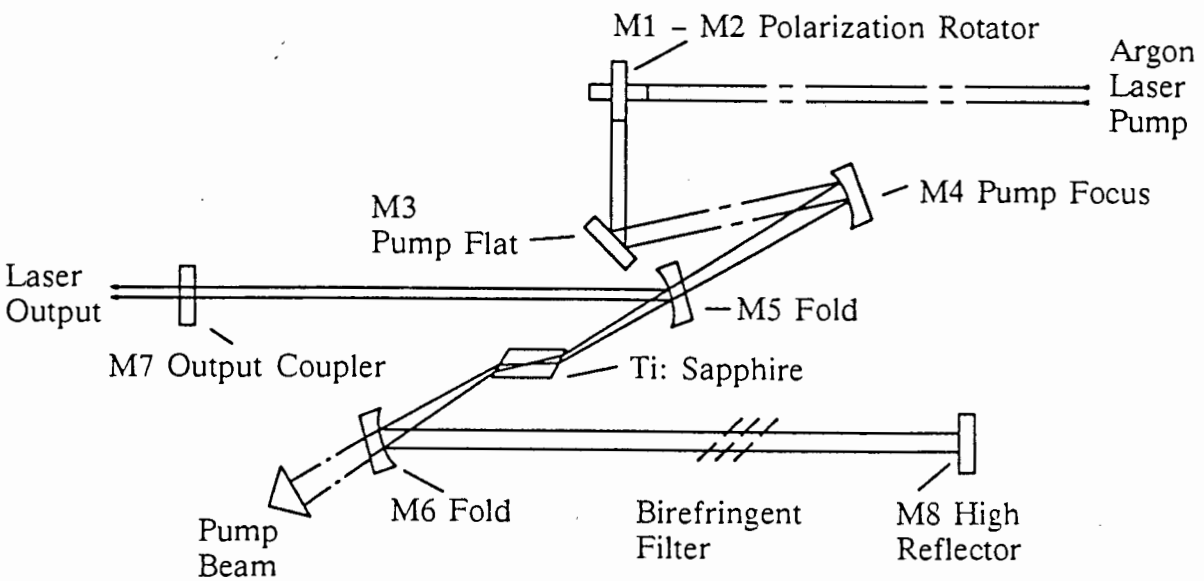

(b)

Fig. 2.1. (a) Typical cw dye laser optical system; (b) Model 3900 cw Ti:Sapphire laser optical system.

PC (propylene carbonate) and 510 ml EG (ethylene glycol) for 1 gram LDS821 dye, which has a tuning range from 780 to 900 nm, covering the near gap region of GaAs.

To improve the spectral width of the dye laser output, we added a birefringent filter, which is made out of four flat and parallel crystalline quartz plates having a total thickness of 14mm [88S].

An alternative tunable laser is Titanium doped sapphire (Ti: Sapphire) as shown in Fig. 2.1b. Ti: Sapphire is a solid-state medium capable of tunable laser action over a broad range of near infrared wavelengths. The broad absorption band in the blue and green make the argon ion laser an ideal pump source for this material. Ti: sapphire eliminates much of the effort required to operate dye lasers in the near infrared, as there are no dyes to change, no circulators to clean and no drop in output power with dye degradation. It can also provide much higher output power than dye lasers.

Ti: Sapphire is a crystalline material produced by introducing Ti_2O_3 into a melt of Al_2O_3. A boule of single crystal material is grown from this melt by one of several techniques. The Ti^{3+} ion is responsible for the laser action of Ti: Sapphire. It substitutes for a small percentage of the Al^{3+}, and the electronic ground state of the Ti^{3+} ion is split into a pair of vibrationally-broadened levels. Absorption transitions occur over a broad range of energies (wavelengths) from 400 nm to 500 nm. Fluorescence transitions occur from the lower vibrational levels of the excited state to the upper vibrational levels of the ground state.

Although the fluorescence band extends from wavelengths as short

as 600 nm to wavelengths greater than 1 μm, the long wavelength side of the absorption band overlaps the short wavelength end of the fluorescence spectrum. Therefore, laser action is only possible at wavelength longer than 650 nm. The tuning range is further reduced by an additional weak absorption band that overlaps the fluorescence spectrum. This band has been traced to the presence of Ti^{4+} ions but it is also dependent on material growth techniques and Ti^{3+} concentration. Finally, the tuning range is also affected by mirror coatings, tuning element losses, available pump power, and pump mode quality. For our study, the Ti:Sapphire laser was optimized for operation in the 700 - 850 nm range.

For continuous-wave (cw) pumping, there is one basic requirement for laser action: the unsaturated round trip cw gain must exceed the round trip loss from all sources. The cw gain is obtained by having a inversion density and a sufficient length of Ti:Sapphire material. A high inversion density in turn comes from having a high pump intensity and a high Ti^{3+} ion concentration. Unlike the dye laser, in which the pump light illuminates a thin dye stream, the pump illumination in the Ti:Sapphire laser must be collinear with the cavity mode over a relatively long length of laser rod. If the typical three mirror cavity used in dye laser (Fig. 2-1a) was used with the Ti:Sapphire, the pump and cavity modes would overlap at one of the fold mirrors, making such alignment difficult. A four-mirror folded cavity is used to allow for tightly focused cavity and pump modes within the laser rod, yet provide a reasonable sized and collimated output beam. In the 3900 model, an additional collimated leg is used and the remaining pump beam

is "dumped" through one of the fold mirrors, resulting in a cavity which is easy to align.

For the time-resolved spectroscopy, a Ar^+-pumped, mode-locked, cavity-dumped dye laser system was employed to generate picosecond laser pulses. This system has been described in detail by Steiner and Charbonneau [86S] [88C], and is capable of delivering a train of laser pulses of spectral linewidth ~0.5meV, time duration ~10ps, and at a repetition rate from single-shot up to 4 MHz.

2.3. Cryostats and Samples

Three different liquid helium cryostats were used for these studies. A standard Janis immersion dewar with optical aperture of f/3 was employed for most cases. For the temperature dependence measurements, an Andonian Variable temperature dewar was used. In this cryostat, a flow of He gas from a reservoir is used to cool the sample. The temperature is sensed by a Si diode sensor (Lakeshore DT-500-CU-36) mounted in close proximity to the samples. The diode signal was monitored by a Lakeshore DRC-80C temperature controller. Temperature control was provided by a heater consisting of resistance wire wrapped around the sample holder.

Magneto-photoluminescence was carried out in a custom built split-pair 10T superconducting magnet cryostat operated in Voigt configuration. The optical throughput is about f/6. In this particular cryostat, the sample chamber is completely separate from the magnet He reservoir. For $T \leq 4.2K$, the sample chamber is filled with liquid He. For temperature above 10K, a crude but effective system is used whereby cold He gas is transferred into the sample chamber using a transfer siphon.

All the semi-insulating GaAs samples (total 1,117 samples) used in this work were provided by Johnson Matthey Electronics Ltd. (formerly Cominco Electronic Materials Ltd.) Trail, British Coulombia, Canada. For the photoluminescence measurements, the samples were mounted on a specially designed holder accomodating up to 20 samples.

2.4. Data Acquisition System

Much of the optical data acquisition apparatus for semiconductors has been described in some detail previously [86S] [86W] [88C] [88S]. A block diagram of the complete experimental apparatus used in most cases of this study is shown in Fig. 2.2.

The photoluminescence was carried out by immersing the samples in liquid helium in a cryostat. The samples were excited using an Ar-ion laser, a dye laser or a Ti:Sapphire laser.

The luminescence was usually detected with a Varian VPM159A3 photomultiplier tube cooled to -100°C. In addition, a liquid nitrogen-cooled intrinsic Ge detector was available for these experiments. This detector does not suffer from the rapid drop in quantum efficiency of the photomultiplier beyond 1.2μm, but for shorter wavelengths it is considerably less sensitive than that device. The PL was dispersed by a 3/4 meter Spex double spectrometer with 600 lines/mm gratings, blazed for 1μm. The maximum resolution of this spectrometer at the GaAs bandgap energy was approximately 0.1meV. In practice, the useful resolution of the system was somewhat less than this, due to a certain amount of jitter in the tracking of the grating mechanism. The photomultiplier signal was digitally processed in a photon counting mode by means of the previously described experimental system.

An IBM-PC computer system provided the capability to do PL spectral scans, in which the wavelength of the spectrometer is advanced by a computer-controlled stepping motor. The system provides the

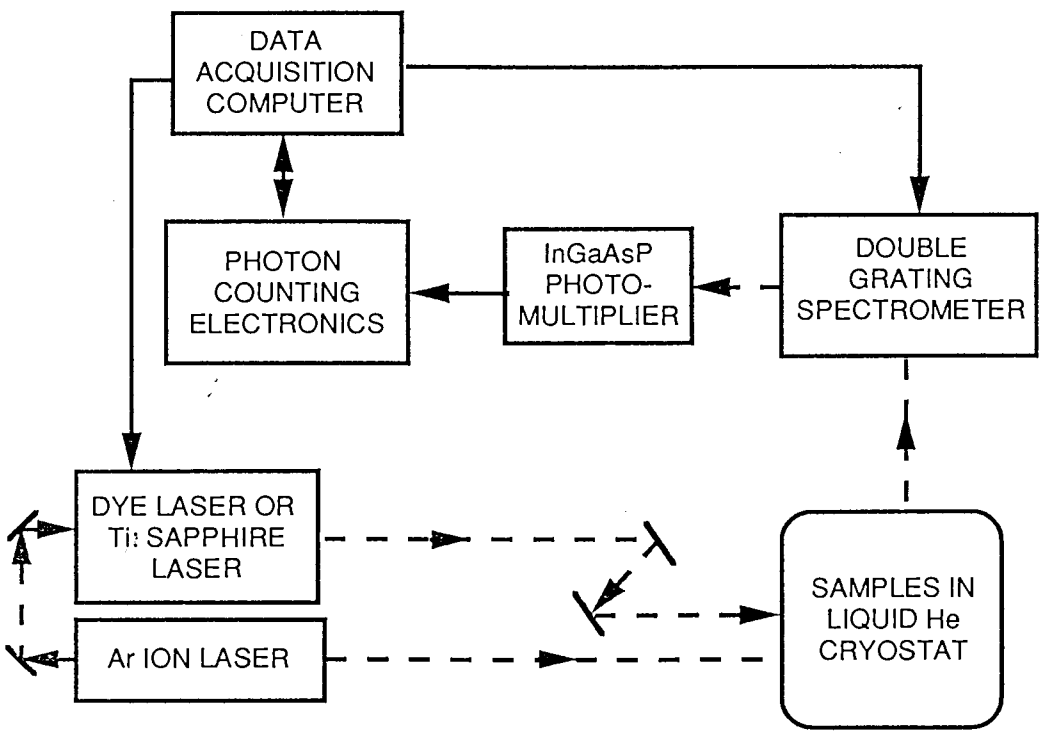

Fig. 2.2. Block diagram of the experimental apparatus.

ability to average successive spectra, in order to improve the signal-to-noise ratio and minimize errors due to drift in either the response of the detection apparatus or the intensity of the laser. By making modifications to the control program, we could use the same program to control the energy of the tunable dye laser or Ti:Sapphire laser.

Time-resolved photoluminescence was performed using single photon counting technique as shown in Fig. 2.3 [86S] [88C]. It used very fast pulse discriminators, together with a time-to-amplitude converter (TAC) which delivers an output pulse to the pulse-height analyzer (PHA), the amplitude of the pulse being accurately proportional to the time difference between the start and stop pulses at the TAC. The pulse-height analyzer (PHA) is then connected to an IBM PC. The computer thus receives a number corresponding to the time difference between the start and stop pulses for each pair of pulses. After the collection of many pairs, a histogram of the luminescence decay was obtained.

The start pulse is generated by the detection of a photon by the photomultiplier tube, which then triggers the constant fraction discriminator. The stop pulses are obtained from a second discriminator which is triggered by a fast Si avalanche photodiode which samples a small portion of the exciting laser beam. At a given wavelength the computer sums the counts in all the channels corresponding to eight separate time windows after the excitation pulse and store the eight sums separately, thus simultaneously collecting eight spectra in different time windows. Alternately, the system can

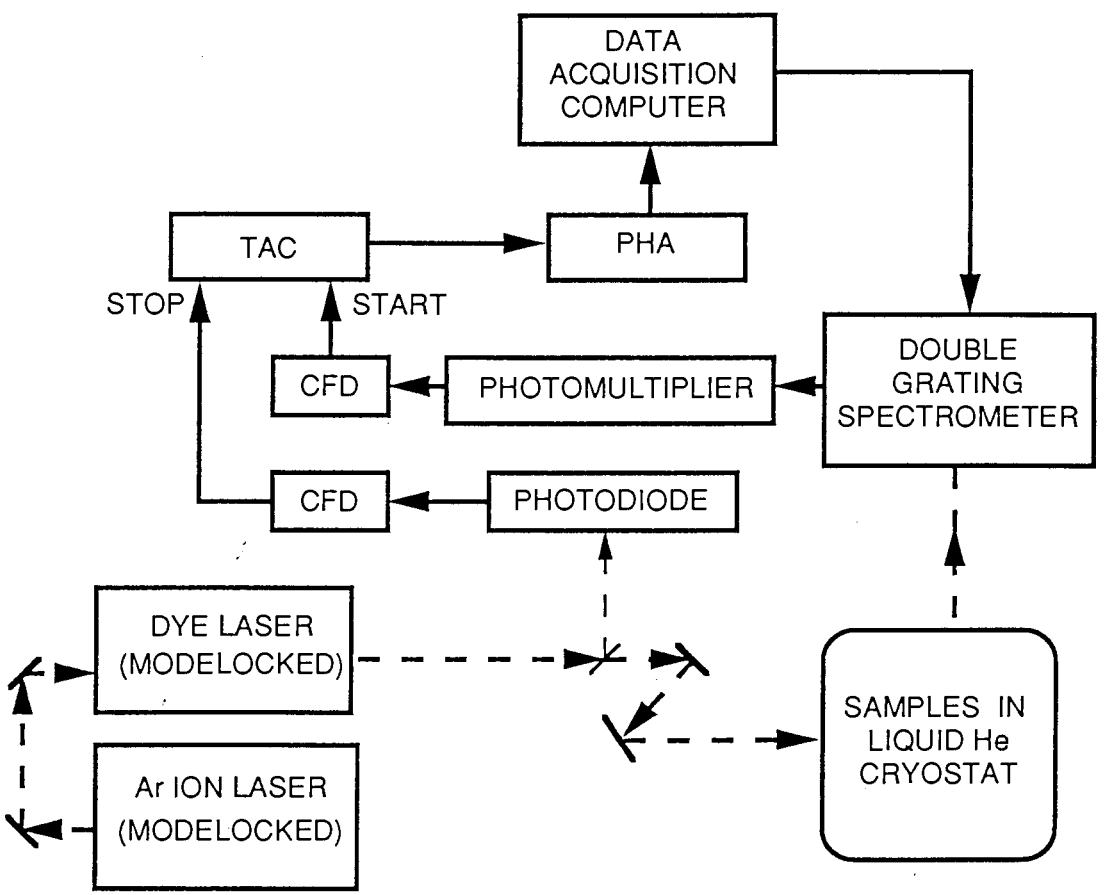

Fig. 2.3. Block diagram of the experimental apparatus for time-resolved photoluminescence using a delayed coincidence photon counting system. PHA: Pulse-height analyzer, TAC: Time-to-amplitude converter, CFD: Constant fraction discriminator.

collect a photoluminescence decay curve at a given wavelength.

CHAPTER 3: IDENTIFICATION OF THE ACCEPTORS

3.1. Introduction

Photoluminescence (PL) is the optical radiation emitted by a physical system resulting from excitation to a nonequilibrium state by irradiation with light. Three processes can be distinguished: (a). creation of electron-hole pairs by absorption of the exciting light, (b). radiative recombination of electron-hole pairs, and (c). escape of the recombination radiation from the sample [72B].

What is the advantage of an experimental technique that involves such a complexity of competing phenomena? Most obvious is the close connection of PL to a number of radiative devices such as the semiconductor lasers, light emitting diodes, and many others. However, photoluminescence is also rapidly evolving into a major research tool comparable in importance to absorption measurements. Two reasons for this stand out as significant. First is the sensitivity of the technique. It often happens that features which are not observable in absorption will completely dominate the luminescence spectra. The converse is also sometimes true, making luminescence and absorption complementary techniques. Second is the simplicity of data collection. Absorption measurements require tedious sample preparation. Samples must be cleaved (or polished) to the proper thickness with parallel (or wedged) front and back surfaces. In contrast, front surface PL measurements can easily be made on bulk materials or thin epitaxial

layers without any sample preparation.

In this chapter, we describe a study designed to improve the usefulness of PL in impurity recognition in GaAs. We realize that the technique is most readily applicable to acceptor identification, since the binding energies of typical shallow acceptors are 5 times those of the donors and the chemical shifts between acceptors, essential for their recognition, are larger still when compared with the donors. The identification of shallow donors in GaAs turns out to be extremely difficult, requiring high magnetic fields, which we will talk about in chapter 5. Besides being used to identify the acceptors, photoluminescence was employed to assess the surface treatment of the samples by measuring the polariton luminescence intensity.

Illuminating GaAs with above band-gap photons photoneutralizes the acceptors and donors as well as creating bound electron-hole pairs or excitons. Generally, non-excitonic processes can be distinguished from exciton luminescence by their broader lineshape and lower spectral energy. In the case of deeper centers, however, it is not always clear which of these possibilities applies.

The technique of photoluminescence excitation spectroscopy (PLE), where the spectrometer is fixed on the luminescence feature and the exciting dye laser (or Ti:Sapphire laser) wavelength is scanned to shorter wavelength, can be used to distinguish whether the luminescence is excitonic and non-excitonic nature. In the case of excitonic luminescence, a PLE peak is observed when the laser is tuned over the exciton-polariton region, thereby resonantly creating exciton-polaritons that are subsequently trapped on impurities. For

non-exciton luminescence the PLE often shows a dip at the energy of the polariton, since the creation of polaritons now creates a parallel recombination path in competition with non-exciton recombination.

Time-resolved spectroscopy is another technique which can provide further evidence to determine whether the luminescence feature is excitonic or non-excitonic. It was found that the luminescence peaks associated with excitons have very rapid exponential decays with lifetimes less than 5ns, while the non-excitonic luminescence peaks have much longer nonexponential decays [69D] [86S] [88C].

3.2. Ordinary Photoluminescence

The chemical identification of impurities and defects by PL relies on the small differences in the binding energy of the electronic particles to the different impurities. The long range component of the interaction is just a Coulomb interaction, and if this were the only contribution all impurities of the same type, i.e., donors (or acceptors), would have the same binding energy. Added to the Coulomb interaction is a short range component called the central cell correction, which is due to interaction with the core electrons and (or) lattice distortions due to the impurity. This additional potential is inherently short range and only affects the energy levels of states which have a significant wavefunction amplitude in the core region, predominantly the 1s level. The central cell potential is responsible for the so-called chemical shifts of the donor and acceptor ionization energies, which permits identification of the different impurities.

Lipari and Baldereshi [70L] have presented calculations of the energy levels of the shallow acceptors in GaAs using the effective mass theory. Because of the core effects giving rise to what are known as central cell corrections or chemical shifts, the ground state which is relatively highly localized suffers greater perturbations and exhibits a greater increase in binding energy than any of the excited states. At present, theoretical treatments of these chemical shifts have not been very successful, and they are best determined by experiment [75A] [86V].

Figure 3.1 displays two distinct groups of features in ordinary photoluminescence with above-gap excitation at 1.8K. The higher energy set of sharp lines includes the polariton (X) at 1515meV, the neutral donor bound exciton (D°,X) at 1514.1meV, the acceptor bound exciton (A°,X) at 1512.34 meV, and sometimes an unidentified bound exciton feature labelled with (?,X) at 1511.04 meV.

The lower energy, broader bands are the donor-acceptor pair band (D°,A°) and the free-electron to neutral acceptor transition (e,A°). The energy of the recombination photon for the donor-acceptor band depends on pair separation due to the electrostatic attraction of the remaining ionized centers as explained previously. The energy of the recombination of a pair separated by a distance R thus increases as R is reduced. Due to this dependence on pair separation, donor-acceptor pair luminescence produces a broad band when non-selective or above band-gap excitation is used. The free-electron to neutral acceptor transition is also broad, due to the initial kinetic energy of the electron. In fact the electron temperature in the crystal can be inferred from a fit to the (e,A) band. In figure 3.1 the highest energy broad band is the free-electron to neutral carbon transition. The next band to lower energy is the overlapping contribution from the neutral donor to carbon acceptor pair band (D°,C°) and the free-electron to neutral zinc acceptor band (e,Zn°), and the other band is the neutral donor to zinc acceptor pair band (D°,Zn°). In figure 3.1a a donor acceptor pair band due to either a Cd or Si is visible. The series of spectra from a to c in figure 3.1 indicate a decreasing concentration of Zn relative to C. In principle the relative intensity

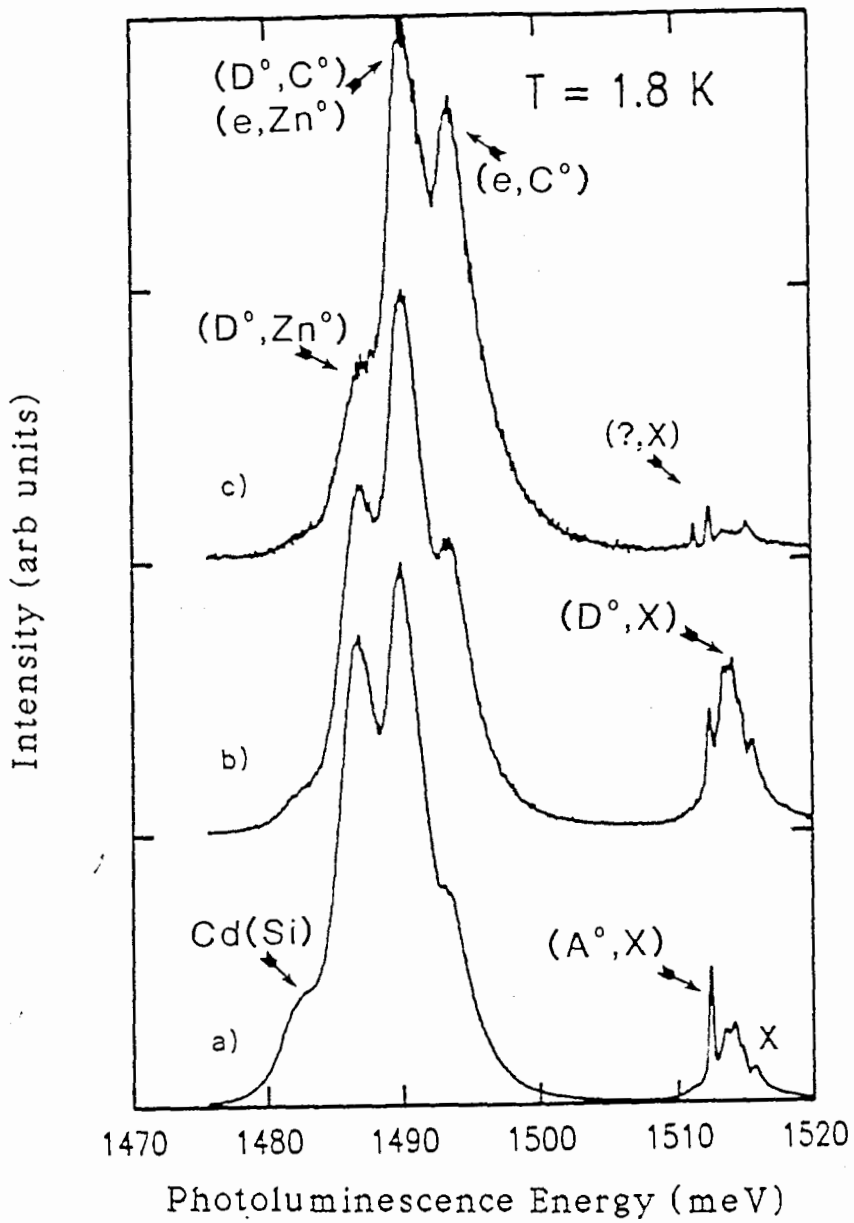

Fig. 3.1. Short-scan photoluminescence with above-gap excitation at 1.8K. (a) shows a relatively strong shallow acceptors (A°,X) while (b) has much stronger shallow donor (D°,X); (c) has a contribution from an unidentified bound exciton labelled with (?,X). Note also the donor-acceptor features with contributions from the various shallow acceptors in different ratios in the three samples.

Table 3.1. Energies of PL lines of shallow acceptors (meV)

Acceptor	free to bound (±0.1)	donor-acceptor pair(±0.1)	bound exciton (1S, ±0.05)
C	1493.5	1490.0	1512.3
Zn	1488.8	1486.0	1512.2 [75A]
Cd	1484.8	1482.5	1512.3 [75A]
Si	1485.0	1482.5	1512.4 [75A]
Ge	1479.0 [83K]		1512.6 [75A]
Mg	1491.1 [85Ka]		1512.4 [75A]

of the donor-acceptor pair to free-electron to neutral acceptor luminescence also contains information on the relative donor to acceptor concentration besides a relative concentration of different acceptors, but in both of these cases it is difficult to extract a reliable, quantitative ratio due to overlapping contributions from different bands. Table 3.1. lists the energies of luminescence lines of shallow impurities.

Deeper impurities, while not as well understood as the shallow effective-mass-like impurities, can also be observed in photoluminescence. Figure 3.2 shows lower energy photoluminescence feature associated with deeper impurities or defects. These tend to form bands that are much broader than features associated with shallow effective-mass-like impurities due to much stronger phonon coupling. Figure 3.2a shows the PL of a sample containing Cu and the donor-accepter pair band (D°,Cu°) at 1360 meV. It should noted that Cu is in general not found in current state-of-the-art as-grown material, but is introduced onto the surface during the etching or polishing phase and then diffuses into the sample during subsequent anneals. LO phonon replicas of the principal features are also seen in figure 3.2. These are characterized by a weaker replicated lineshape separated from the principal line by the 36.3meV LO phonon energy of GaAs. Several other peaks are also visible; the one at 1405meV labelled (Mn°,X), while at the energy usually associated with a Mn donor acceptor pair, is not , however, a donor-acceptor band as determined by excitation spectroscopy which will be discussed in section 3.3. Figure 3.2b shows a peak labelled Ga_{As} for the Ga antisite double acceptor in GaAs [86V].

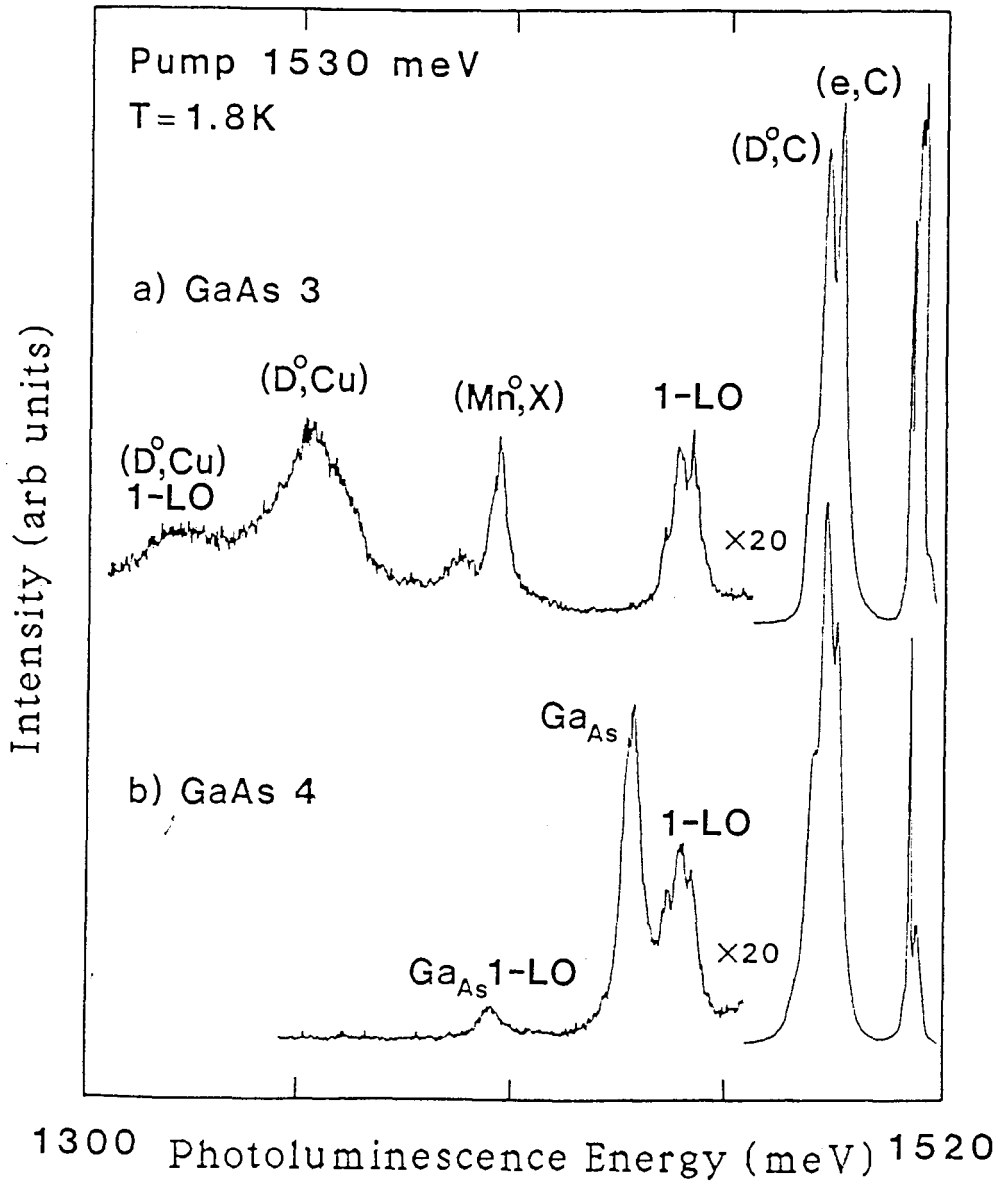

Fig. 3.2. Long-scan photoluminescence for deeper binding centers. In (a) the Cu DAP band as well as the shallow acceptor DAP band and their LO phonon replicas are visible. Also in this sample there is a Mn related BE feature labelled (Mn°,X)?. (b) A sample grown under Ga rich conditions has a characteristic DAP band from the Ga antisite double acceptor.

The main photoluminescence line energies of deep acceptors which are detected in this work are given in table 3.2. For the emission peaks which were already reported by other authors, the most probable identities of the responsible emission centers are included in the Table. The PL lines related to Ga_{As} and Cu_{Ga} can be attributed to band-acceptor (e,A^{o}) and donor-acceptor (D^{o},A^{o}). These are unresolved in the present work due to the relatively high impurity content of the crystals studied which causes both a broadening of emission lines and a decrease in energy difference between (e,A^{o}) and (D^{o},A^{o}) luminescence maxima. Our recent study shows that Mn_{Ga} behaves like a bound exciton and the peak labelled U is undetermined [75A], which we will discuss in later section.

Table 3.2 PL Emissions for deep acceptors (meV)

PL energy (±0.5)	Identity	Reference
1477	U (Ge_{As}?)	[75A]
1441	Ga_{As}	[86V]
1405	(Mn,X)?	[80K]
1360	Cu_{Ga}	[86V]

3.3. Photoluminescence Excitation Spectroscopy

In order to distinguish exciton from nonexciton luminescence, we employed photoluminescence excitation spectroscopy, by observing whether there is a peak (exciton) or a dip (non-exciton) in the PLE signal as the dye laser is tuned to resonance with the polariton. Figure 3.3 shows PLE spectra of the principal PL features displayed in figure 3.2. Figure 3.3a is the PLE spectrum of the carbon donor-acceptor peak labelled (D^o,C^o) in figure 3.2. Note in particular the dip observed at the energy of the polariton labelled X in the figure: this clearly identifies this band as a donor-acceptor band. Also visible is the structure labelled SPL due to the resonant creation of donor-acceptor pairs with the acceptor in various excited states, which we will explain in detail at chapter 4. The origin of the broad band to lower energy has not been determined but is nonresonant in nature as evidenced by its width.

Figure 3.3b shows a similar PLE spectrum of the Cu related emission observed in figure 3.2. It also has a dip at the polariton energy, identifying it as donor-acceptor pair recombination. The SPL structure in this case is smeared out and individual excited states cannot be resolved.

The observed peak at 1405meV, which on the basis of its energy position would have been assigned to Mn acceptor related donor-acceptor pair band, does not have a dip in its PLE spectrum in figure 3.3c. instead, this feature has a peak at the polariton position, indicating that this is bound exciton luminescence. The

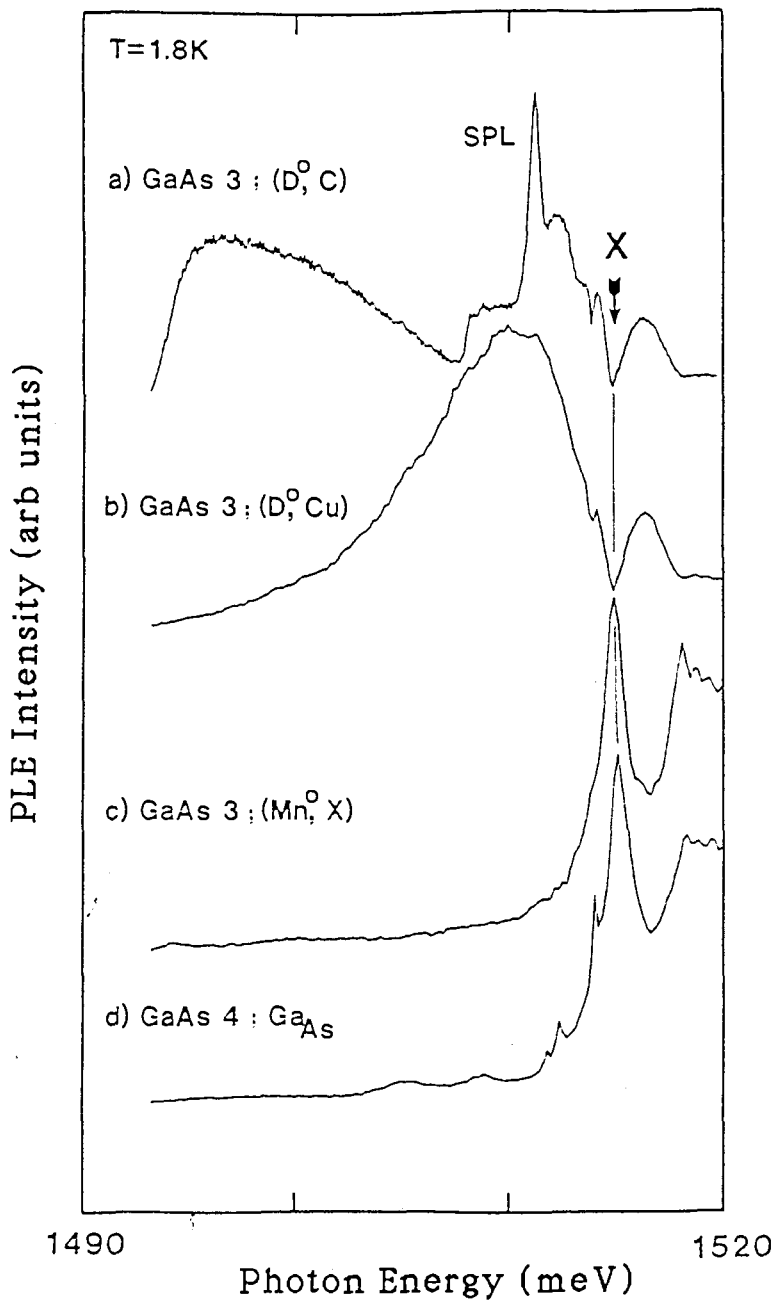

Fig. 3.3. PLE spectra of the samples in Fig. 3.2 confirming the assignment of the peaks in Fig. 3.2. DAP bands have a dip at the polariton energy labelled X while BE have a peak at the polariton energy. The spectrometer is set at the peak of the labelled feature while the excitation energy is scanned.

time-resolved experiments (not shown) independently confirmed the bound exciton feature of this transition. It is thus unlikely to be the same peak referred to by the references on Mn in GaAs. Its origin, other than the fact that it is a deep bound exciton, is at the moment unresolved.

The PLE at figure 3.3d of the 1441 meV Ga_{As} peak observed in figure 3.2. has a peak at polariton energy, confirming the bound-exciton character of this peak.

Figure 3.4 displays the photoluminescence spectra of two samples in the near-gap region, while figure 3.5 shows the corresponding PLE spectra of the various observed lines, Note that the lines (?,X), (C^{o},X) and U are all bound exciton features while (D^{o},C) and (D^{o},Zn) show PLE spectra characteristic of donor-acceptor pair luminescence as expected. The only surprise here is the nature of the U luminescence, which due to its spectral position and width was initially assumed to be donor-acceptor pair luminescence due to Ge acceptors, which are expected to have a peak in this energy region. The identification of the U line, only observed in two samples, remains undetermined. The above samples indicate the importance of the PLE in the identification of the luminescence features and the danger of relying solely on the PL energy position of the feature for their identification.

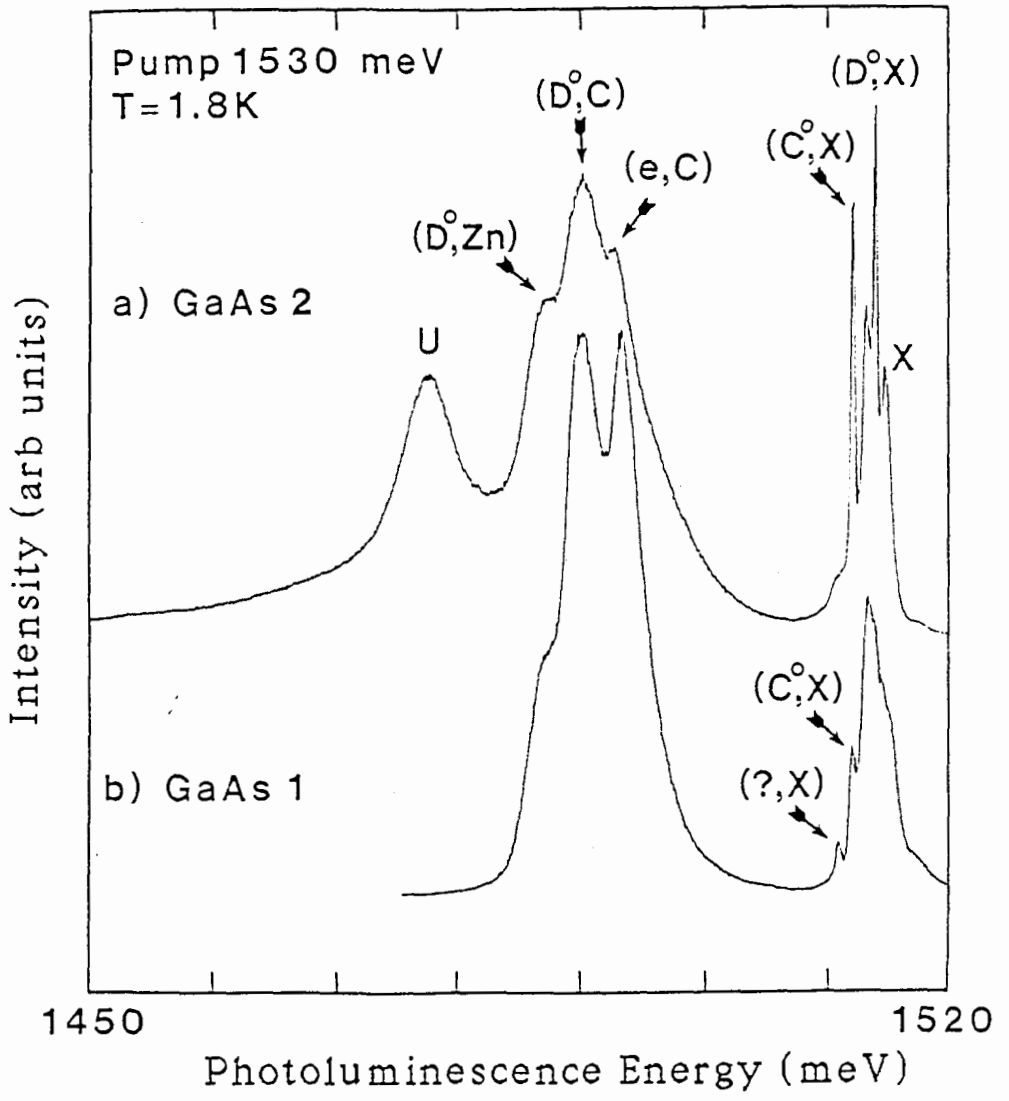

Fig 3.4. PL spectra from two samples showing spectral feature of unknown origin. Sample (a) has a broad band labelled U that, although at the position of the Ge acceptor DAP band, is actually like a BE feature despite its width; (b) shows a BE slightly below the usual (C°,X) labelled (?,X).

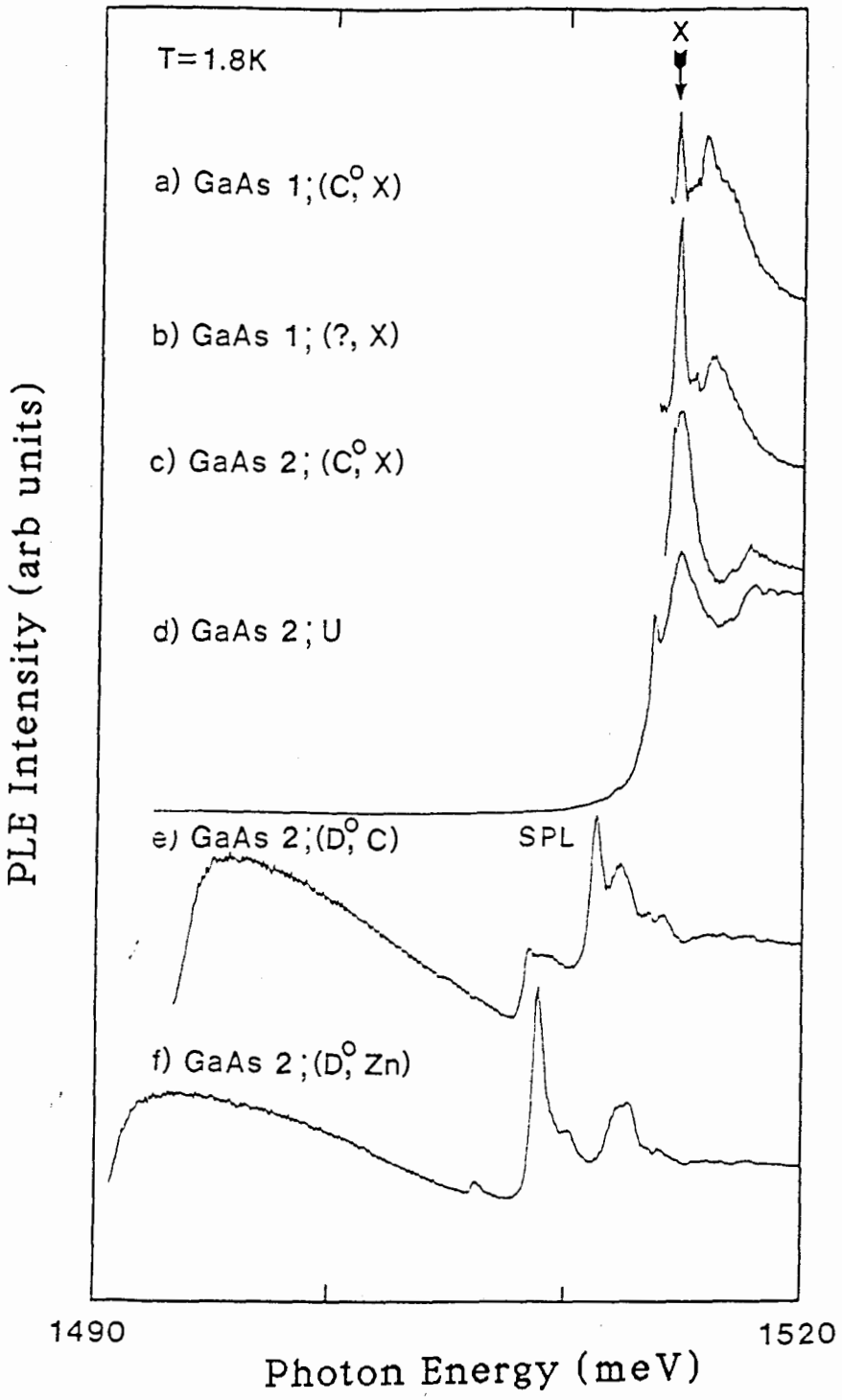

Fig. 3.5. PLE spectra of various feature in the spectra displayed in Fig.3.4. confirming U and (?,X) at luminescence (a)-(d) might be BE feature since they have a peak at polariton energy while the DAP luminescence feature (e) and (f) have a dip.

3.4. Time-resolved Photoluminescence

A series of time-resolved spectra of semi-insulating sample GaAs-2 using above gap excitation are shown in Fig. 3.6. The sample is immersed in superfluid helium and the luminescence is excited using the mode-locked, cavity-dumped dye laser system described in chapter 2. The luminescence is dispersed by a double grating spectrometer, detected by the photomultiplier, and analyzed by the computer system. The top spectrum is a regular CW photoluminescence scan. The time window used for the acquisition of the spectra varied from 10ns (for the second top spectrum) to 60ns (for the bottom spectrum). This series of spectra clearly show that the neutral acceptor bound exciton (A°,X), neutral donor bound exciton (D°,X), and polariton lines in the exciton range labelled with X decay much more quickly than the lower energy donor acceptor pair (D°,C°), (D°,Zn°), and free-to-bound (e,C°) lines labelled with DAP. For the unidentified peak labelled with U, the life time measurement shows that it is more like a donor acceptor pair with longer life-time.

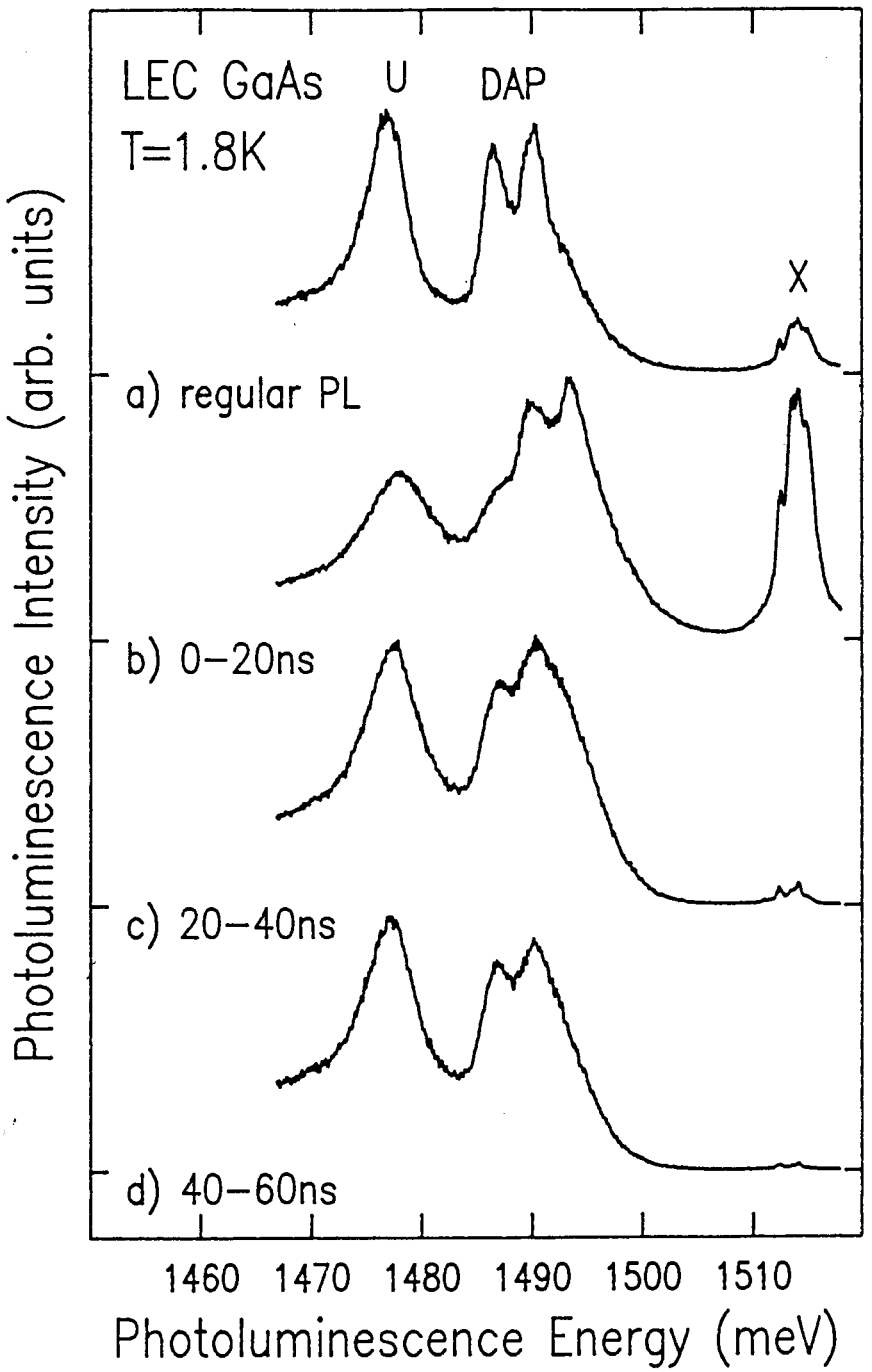

Fig. 3.6. Time-resolved photoluminescence measurements. The top spectrum is regular PL, while the time-windows for (b)-(d) are as indicated on the figure. The sample was excited by 814 nm radiation at a repetition rate of 4Mhz with an average excitation density of 50 mW/cm^2.

3.5. Polariton Photoluminescence

Since GaAs is a direct-gap semiconductor, free excitons couple strongly to photons and the correct description of the excitation is a mixed exciton-photon mode known as a polariton. There is a population of polaritons that can only yield external luminescence if the excitation first travels to the surface. In the polariton picture, a polariton impinging on the crystal interface has a certain probability of being transmitted as a photon and a certain probability of being reflected back as a polariton. The polariton luminescence process must thus be viewed as a transport process of the polaritons to the surface of the crystal. The oscillator strength of the polariton luminescence is thus not an intrinsic property of the crystal but instead depends strongly on scattering mechanisms and surface quality.

The nature of the polariton luminescence process can be used to evaluate sub-surface damage caused by, for example, mechanical polishing [89S] [89M]. Figure 3.7 shows the results of photoluminescence scans of the exciton region of the adjacent samples subjected to progressively longer etches. The four spectra are from samples cut from the same polished wafer and then etched to different depths. The bottom spectrum is that of an unetched mechanically polished surface and shows a negative polariton peak. The polariton photoluminescence evolves from a dip to a peak as more of the damaged surface is removed. The interpretation is that the near surface damage scatters or absorbs the polaritons, preventing them from reaching the surface and contributing to the sample luminescence. As the damaged

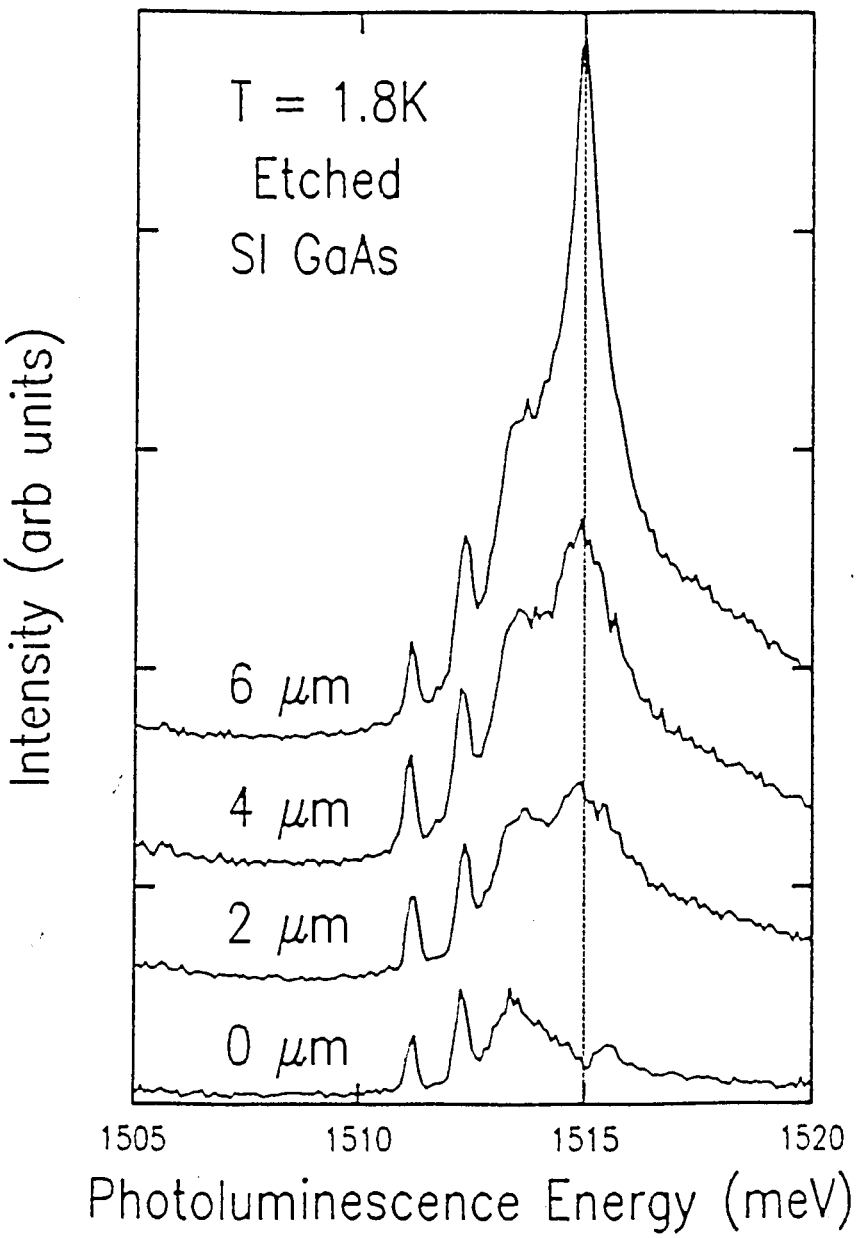

Fig. 3.7. The effect of near surface damage on the polariton PL is evident by the dramatic change in polariton intensity after etching. The sample labelled 0 μm is an unetched sample and the other are neighboring samples etched to the depths indicated in the figure.

region is progressively removed, the polariton intensity steadily increases as the probability of reaching the surface and being transmitted as external photons increases.

3.6. Conclusion

Photoluminescence, photoluminescence excitation spectroscopy, and time-resolved photoluminescence have been employed to investigate the acceptors which are related to C, Zn, Cd(Si), Ga_{As}, Mn, and Cu in semi-insulating GaAs. The unidentified peaks at 1511.04meV labelled with (?,X) and 1477meV labelled with U have also been reported.

For the deep acceptors it is perfectly adequate to use ordinary photoluminescence to differentiate between the chemically distinct impurities and complexes, but this task is more difficult for the shallow effective mass acceptors due to their small chemical shifts.

The photoluminescence peaks at 1441, 1405, and 1360 meV correspond to Ga_{As}, Mn, and Cu as reported. The photoluminescence excitation spectroscopy shows that the peaks at 1405 and 1441 meV are bound exciton features while the peak at 1360 meV is a donor-acceptor pair luminescence. For the peak at 1477 meV, PLE measurements suggest a bound exciton origin while time resolved results suggest a DAP transition.

The polariton photoluminescence has been used to qualitatively evaluate subsurface damage caused, for example, by mechanical polishing. The near surface damage scatters or absorbs the polaritons, preventing them from reaching the surface and contributing to the sample luminescence. As the surface damage is etched, the polariton photoluminescence intensity steadily increases.

CHAPTER 4: SELECTIVE DONOR-ACCEPTOR PAIR LUMINESCENCE

4.1. Introduction

As we discussed in chapter 3, it is perfectly adequate to use regular photoluminescence to distinguish the deep acceptors in semi-insulating GaAs, but this task is more difficult for the shallow effective mass acceptors due to their small chemical shifts. The various donor-acceptor bands and free-electron-acceptor bands, while separated by the full chemical shift, have the drawback of being broad and hence overlapping.

Selective donor-acceptor pair luminescence (SPL) is a low temperature photoluminescence process which involves the resonant excitation of pairs of donor and acceptor impurity atoms separated by a particular spatial distance and can therefore get the full chemical shifts with narrow line width. SPL has been shown to be a very useful technique to monitor the shallow acceptors in GaAs with high sensitivity and high resolution, particularly in samples with low impurity concentrations [88I] [82Ha] [83K].

In order to analyze the impurities quantitatively, it is necessary to understand the effect of the excitation conditions on the SPL spectra. In this chapter, we discuss the dependence of SPL on the excitation energy, excitation intensity, impurity concentration, and temperature in semi-insulating GaAs. It has been suggested that electronic Raman scattering is useful for quantitative analysis of shallow acceptors in semi-insulating GaAs [86Wa] [85W] [84H]. For

comparison, the electronic Raman scattering experiments are also performed.

4.2. Principle

The principle of this experiment relies on the fact that the donor-acceptor pair transition energy is a function of the separation between the donor and acceptor, due to the Coulomb interaction between the impurities. A tunable excitation light source at an energy below the band-gap energy creates an electron on a donor and an excited hole on a nearby acceptor. If the hole relaxes quickly to its ground state, it can recombine with the donor electron emitting a photon with the energy shift between the incident and the emitted photons which allows accurate determination of the excited state position.

The energy required to create the pair with an excited hole is [85Ka]:

$$h\nu_{ex} = E_G - E_A^* - E_D + e^2/\varepsilon R^2 + J^*(R) \qquad (4.1)$$

where E_G is the band gap, E_A^* is the energy of the excited hole with respect to the valence band, E_D is the energy of the donor electron with respect to the conduction band, $e^2/\varepsilon R^2$ is the Coulomb attraction of the ionized centers at distance R from one to another, and $J^*(R)$ represents the interaction of the donor and excited acceptor wave function. When a donor-acceptor pair is created, the energy of the emitted photon is

$$h\nu_{em} = E_G - E_D - E_A + e^2/\varepsilon R^2 + J(R) \qquad (4.2)$$

where E_A is the energy of the ground state of the hole with respect to

the valence band, and J(R) represents the interaction of the donor and the ground state acceptor wave function. From (1) and (2), the energy shift between the excitation and emission photons is given by

$$h\nu_{ex} - h\nu_{em} = - (E_A^* - E_A) + (J^*(R) - J(R)) \qquad (4.3)$$

In principle, pairs should be created with donor electrons in excited states as well, but peaks due to this process are not observed. The first excited state of the donor is only 1.5meV from the band edge and these weakly bound states may be thermally ionized with high probability. Furthermore, due to the very extended wave function of the excited donor, the energy levels may be substantially broadened by interaction with other defects. This may make the SPL peaks for excited donor states too wide to resolve.

4.3. Experimental results

Excitation is provided by an Ar-ion laser pumping a dye laser or CW Ti: Sapphire laser as we described in section 2.2. The laser beam is focused onto a sample to a 2 mm^2 spot. The samples are immersed in liquid helium which can be pumped below the lambda point in a cryogenic dewar. The emitted light is analyzed by scanning a double grating spectrometer and detected with a InGaAsP photo-multiplier tube.

Figure 4.1 shows the excitation energy dependence of SPL spectra recorded at 1.8K. The 10mW/mm^2 excitation is varied from 1506 meV to 1514 meV. The top and bottom spectra are almost typical of the broad PL observed when the sample is excited by above bandgap energy so that they are non-resonant PL peaks. The resonant peaks are the SPL peaks which shift with the excitation energy. For the SPL peaks the energy shift between the excited and emitted photons is equal to that between the excited state and the ground state of the acceptor level for large R, that is [88I]:

$$h\nu_{ex} - h\nu_{em} = -(E^{*}_{A} - E_{A}) \qquad \text{for large R} \qquad (4.4)$$

A series of sharp SPL lines corresponding to individual transitions are observed. Nine peaks are apparent which remain at nearly constant energy shifts from the laser. Three main intense peaks which are located at 18.5, 21.5 and 25.3 meV below the laser are identified as C_{1s-2s}, Zn_{1s-2s}, and $Cd(Si)_{1s-2s}$ [82Ha] [83K]. The less intense peaks correspond to the 1s-2p difference of C, Zn, and Cd(Si). The Cd and Si acceptors have almost identical central cell potentials so that they

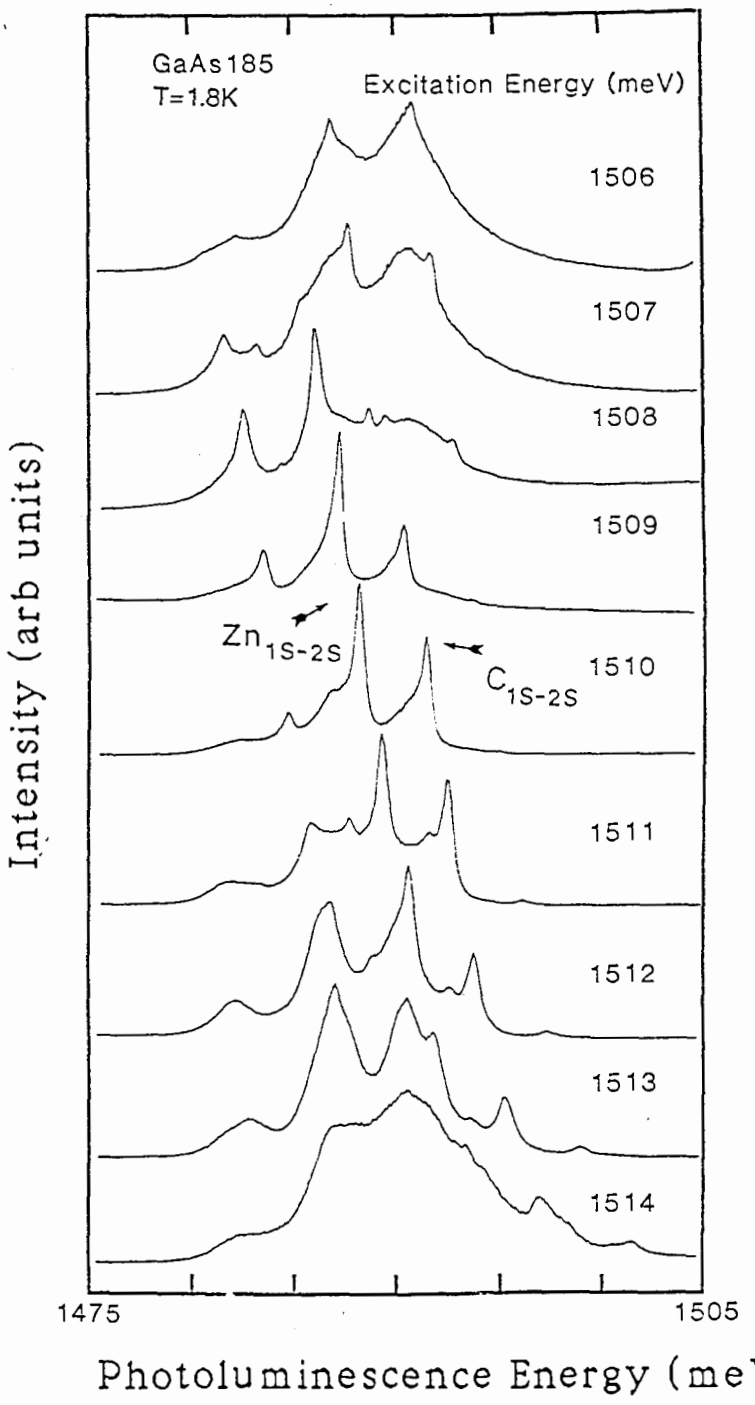

Fig. 4.1. The excitation energy dependence of SPL spectra from 1506 to 1514 meV with 10mW/mm^2 at 1.8K. The resonant peaks are the SPL peaks which shift with the excitation energy. The top and bottom spectra are nearly non-resonant PL peaks.

cannot be resolved using this technique.

The intensity dependence of three main peaks as a function of photoluminescence energy is given in figure 4.2. This information is used to resolve possible ambiguities in acceptor identification in the multiple acceptor case. The main difficulty to make this figure is to separate the non-resonant and resonant PL contributions. The SPL peaks for C_{1s-2s}, Zn_{1s-2s}, and $Cd(Si)_{1s-2s}$ correspond to 1491, 1488.5 and 1483.2meV, which are located at 18.5, 21.5 and 25.3meV below the laser accordingly. Thus, the best excitation energies for these peaks correspond to 1509.5, 1510, and 1508.5 meV. The half-intensity-width of these SPL peaks is about 2.5meV.

Fig 4.3 shows the excitation intensity dependence of SPL spectra. Using 1510meV excitation energy at 20K temperature, we changed the excitation intensity from 25mW to 0.1mW on a $2mm^2$ spot. When the excitation intensity is decreased, the SPL peaks become sharp and the signal to noise ratio is good even at very low excitation intensity. From this fact, it is possible to observe the SPL peaks in high concentration samples ($>10^{16}cm^{-3}$) with low excitation intensity.

The spectral shape of SPL strongly depends on the impurity concentration. Figure 4.4 shows the SPL spectra at different carbon concentrations. As the carbon concentration increases, the SPL peaks of carbon become broad and weak and the non-resonant band becomes broad and shifts to the lower energy side. When the acceptor concentration increases, the separation between acceptors decreases obviously. The recombination probability increases as the separation R decreases because the probability W for DAP recombination is given by [65T]:

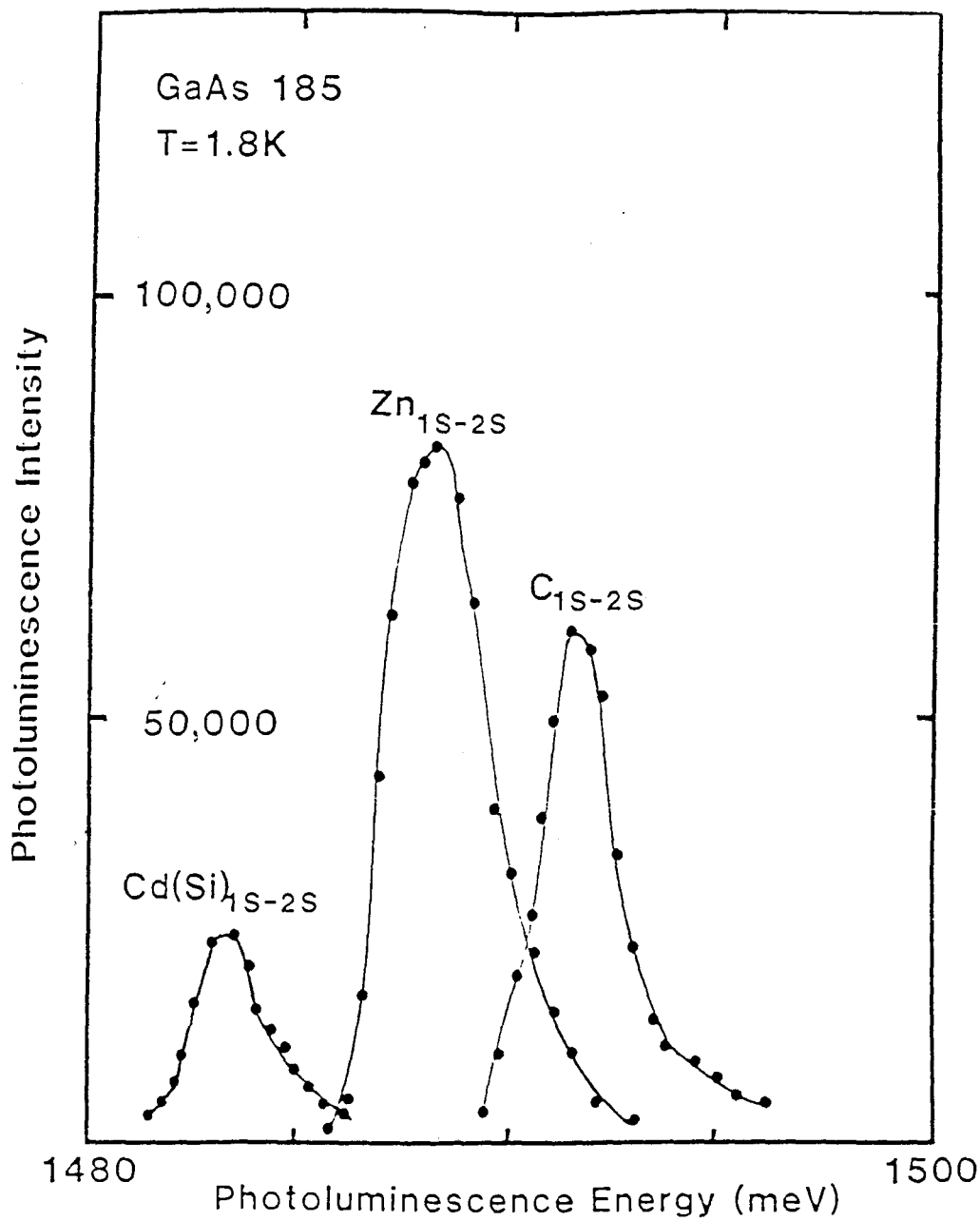

Fig. 4.2. The intensity dependence of SPL peaks as a function of photoluminescence energy for the sample GaAs 185 according to the Fig. 4.1.

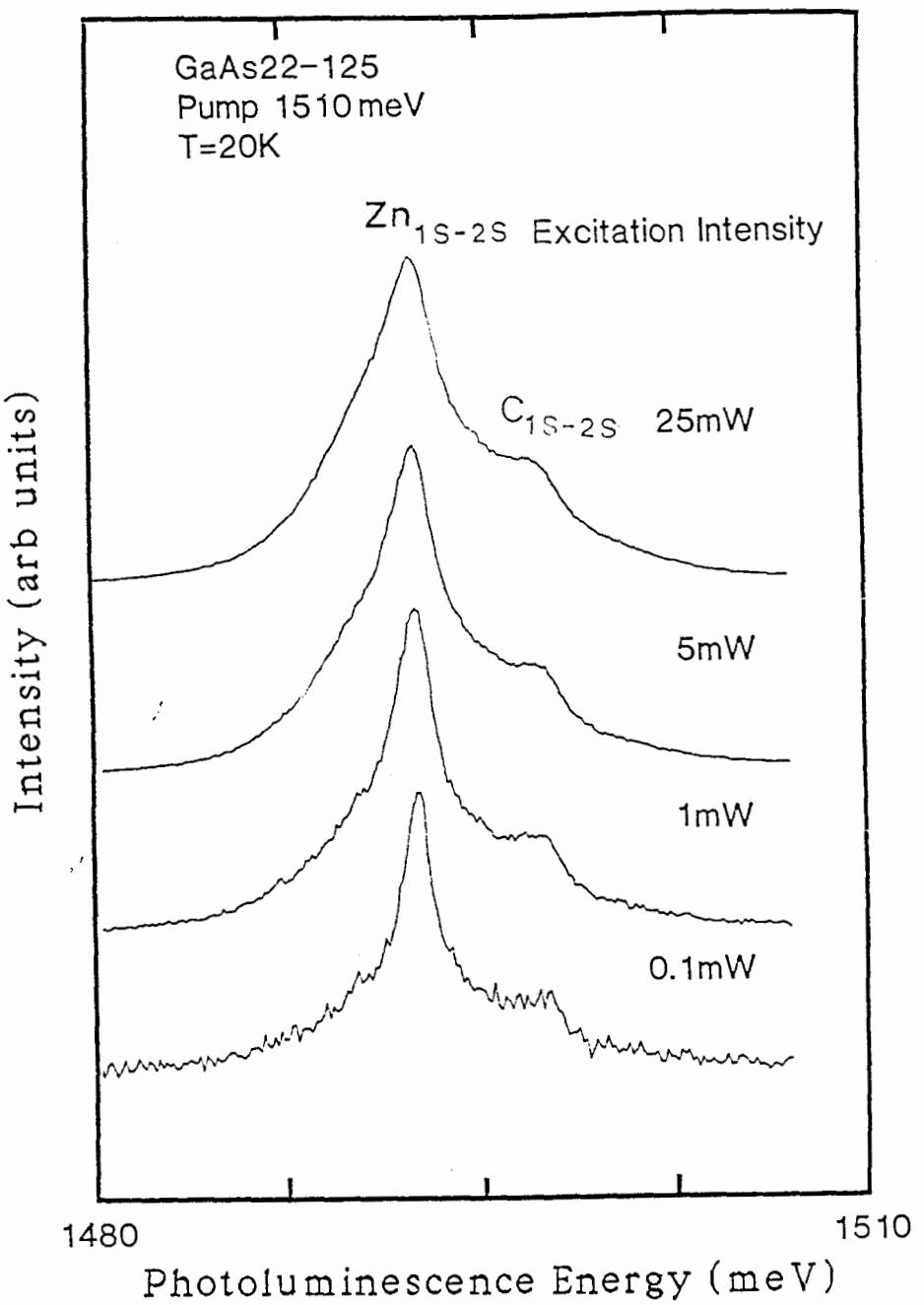

Fig. 4.3. Variation of SPL spectra with the excitation intensity from 0.1mW to 25mW on a $2mm^2$ spot using 1510meV excitation energy at 20K. The SPL spectra become sharp as the excitation decreases.

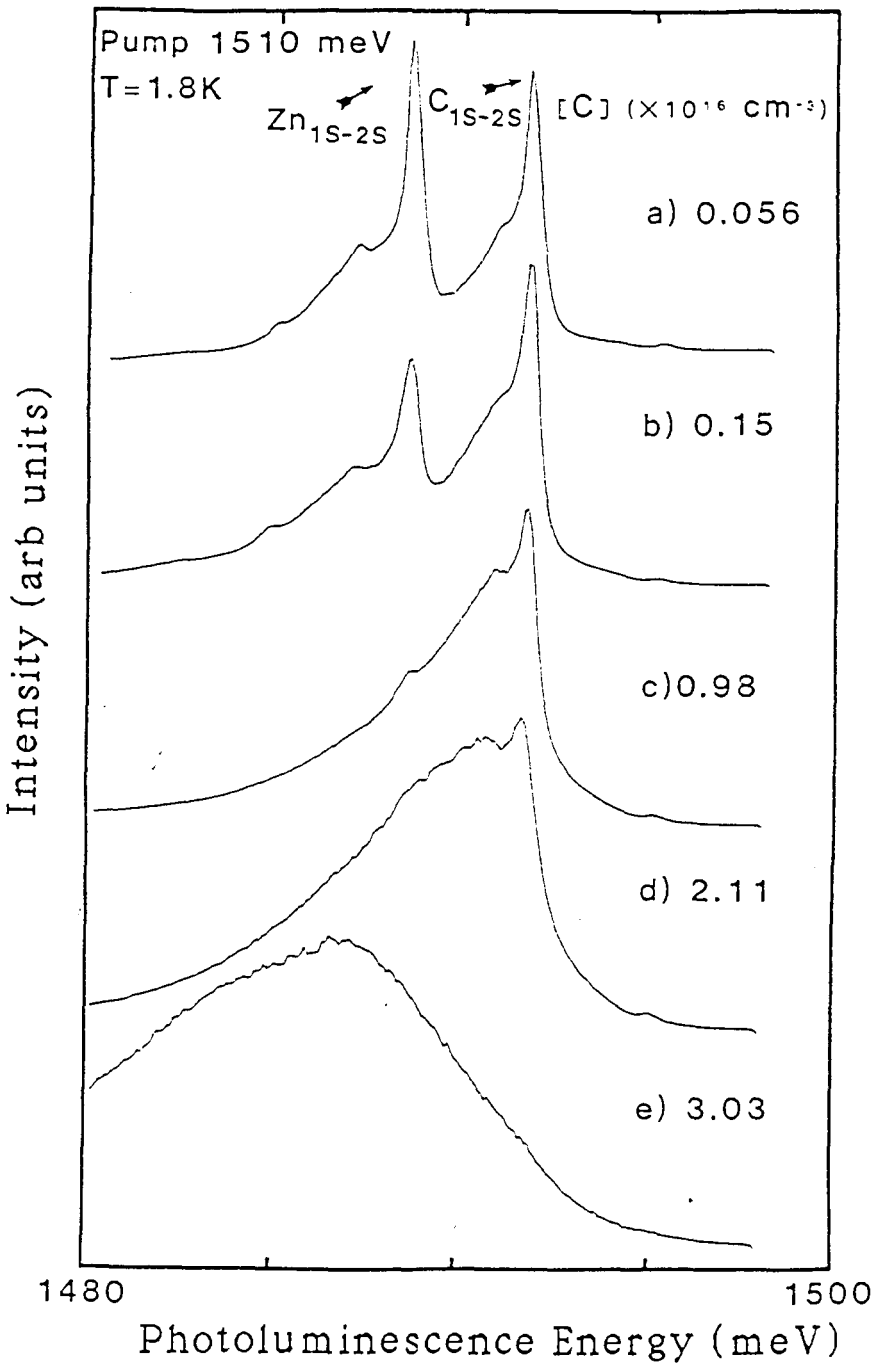

Fig. 4.4. Dependence of SPL spectra on carbon concentration from 0.056 to $3.03\times10^{16}cm^{-3}$. The SPL peaks become broad and weak as the carbon concentration increases.

$$W = W(0)\ \exp(-2R/a_0) \qquad (4.5)$$

where W(0) is a constant, and a_0 is the donor Bohr radius. In GaAs, a_0 is about 74 Å [88I]. When the recombination probability of SPL is small enough compared to the non-resonant peaks which locate in the same range of SPL peaks, the non-resonant peaks are more intense than the SPL peaks, resulting in the SPL peaks unresolved.

Figure 4.5 shows the evolution of SPL spectra with temperature. An Andonian variable temperature dewar was used here while the optical system was the same as above. From 1.8K to 20K, there is no significant change in the relative intensities of two main SPL peaks. A sudden decrease in intensity of the SPL peaks occurs between 20-30K and the resolution between C and Zn peaks is lost. We also observed the PL energy shifts slightly toward higher energy as a function of temperature due to an increasing recombination of more closely spaced donor-acceptor pairs.

When the temperature increases, electrons are released from their donor sites. Therefore, the donor-acceptor pair recombination is quenched and the intensity of SPL peaks is reduced. The released electron may also find its way to another donor site. As the radiative lifetime for this process increases with the donor-acceptor separation, the increasing in temperature results in a reduction of average lifetime and consequently in an increase in the average Coulomb energy contribution to photon so that the donor-acceptor peak shifts towards higher energy.

In fig. 4.6, SPL spectra of a series of nonproduction experimental samples are displayed. Sample a contains predominantly Zn, sample c

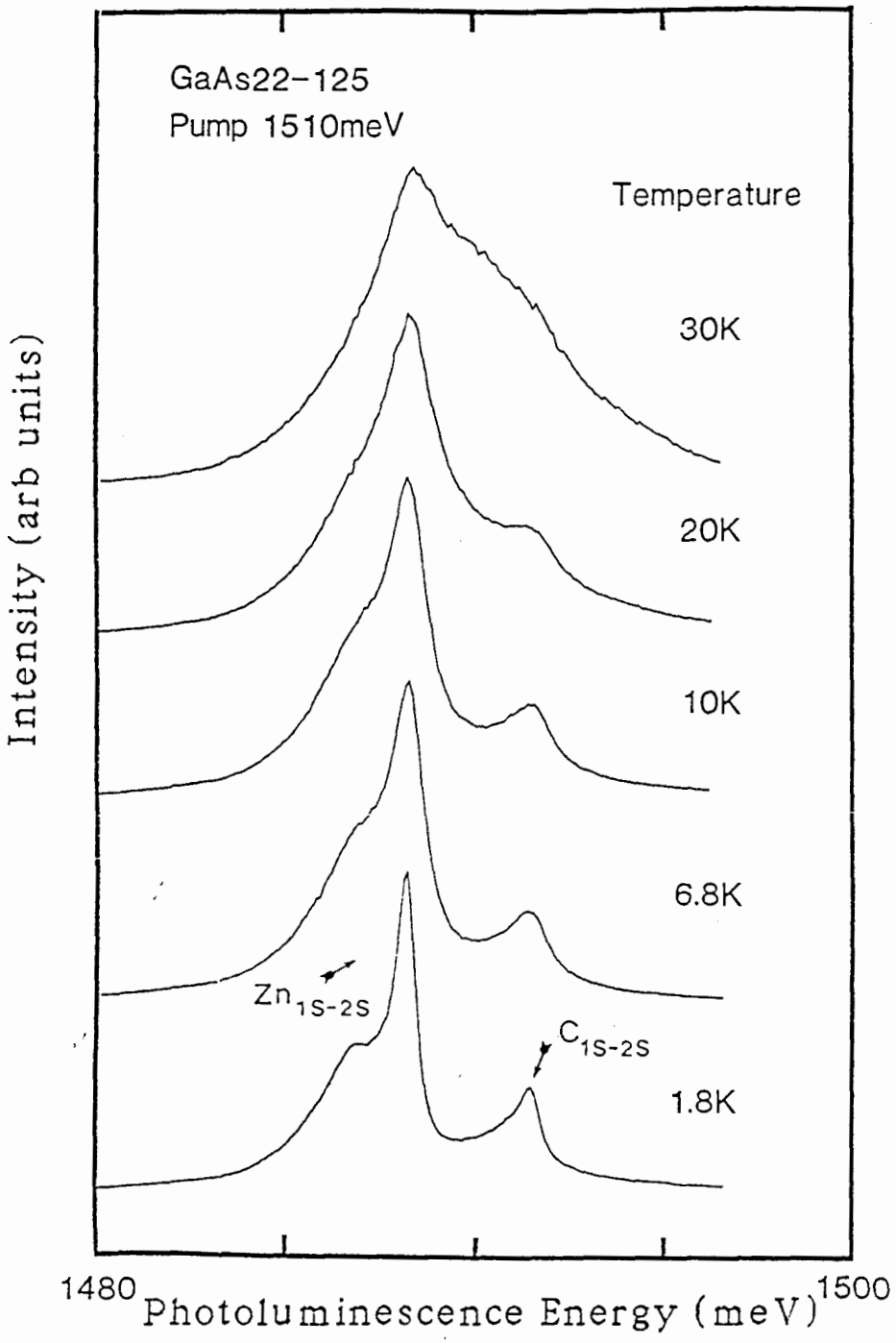

Fig. 4.5. Evolution of the SPL spectra with temperatures from 1.8K to 30K. The relative intensities of C and Zn peaks do not have much change from 1.8K to 20K. A sudden decrease in the intensity of the SPL peaks between 20-30K occurs and the resolution between C and Zn peaks is lost.

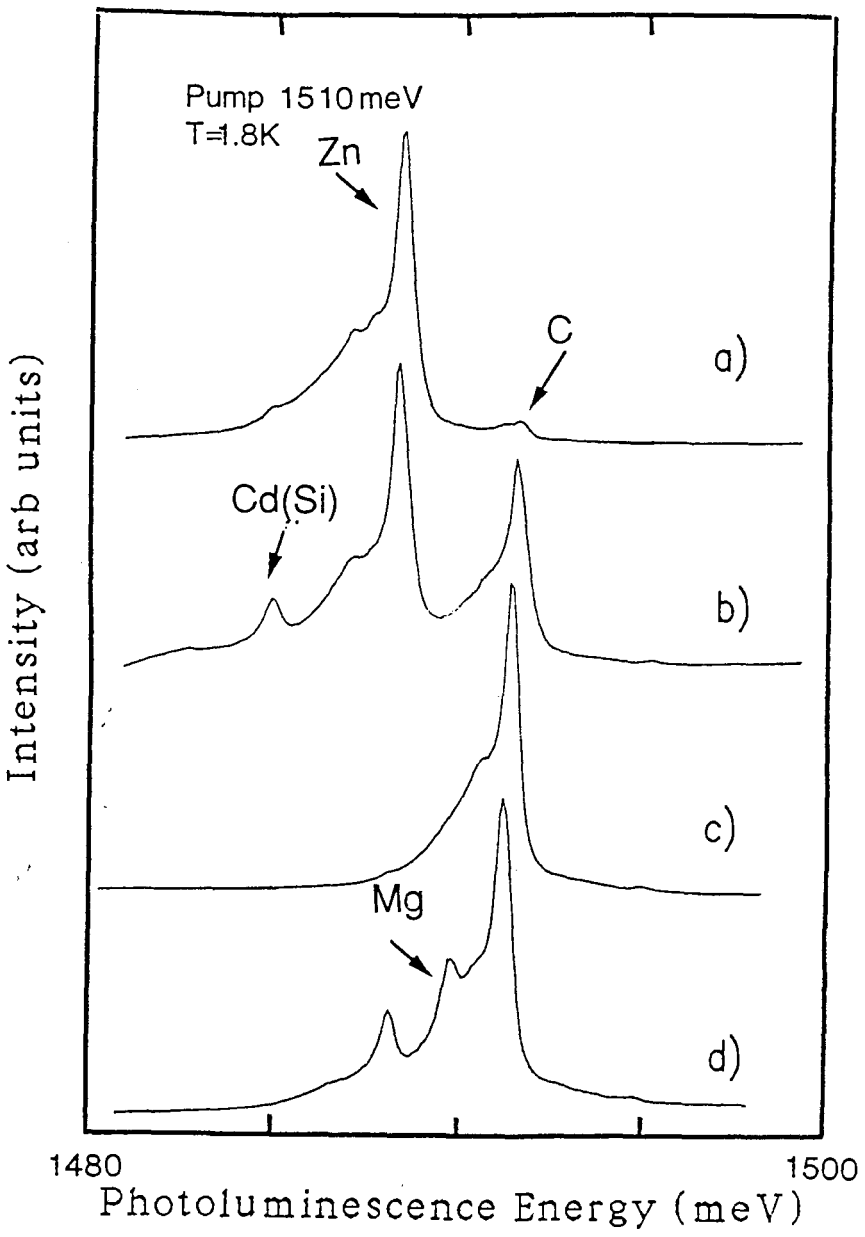

Fig. 4.6. SPL spectra of a number of interesting samples. (a) contains predominantly only Zn, (b) contains Si(Cd) besides C and Zn, (c) contains predominantly C, (d) has a contribution from Mg, which has not been reported before.

contains predominantly carbon, sample b contains a contribution either from Cd or Si besides C, Zn. Figure 4.6(d) shows a Mg peak, which has not been reported before in SPL. The results from SPL measurements are summarized in Table 4.1.

The SPL technique also has very good reproducibility in our experiments. At the same excitation energy and intensity, we have obtained very similar SPL spectra for the sample GaAs 22-125 (used as a reference sample) forty-two times on different days in two years. This is primarily because SPL is not strongly dependent on excitation intensity at liquid He temperatures.

Table 4.1 Excited states of shallow acceptors (meV)

	C	Zn	Cd(Si)	Ge	Mg	
$1S_{3/2}$	26.0	30.7	34.5	40.0		a
$1S_{3/2}$- $2S_{3/2}$	15.2	19.2	23.5	26.1		a
	15.08	19.25	23.75			b
$1S_{3/2}$- $2S_{3/2}$	18.4	21.7	25.1	28.3	20.1	a
	18.5	21.65	25.3	28.25	20.5	b
$1S_{3/2}$- $2P_{5/2}$	19.4	23.1	27.3	30.1		a
	19.42	23.06	27.5	30.0		b
$1S_{3/2}$- $3S_{3/2}$	22.4	26.2	30.8	34.0		a
	25.8					b

a. references [83K] and [85Ka] b. this study (±0.05meV)

4.4. Comparison of SPL with Raman scattering

An alternative method of acceptor identification uses electronic Raman scattering (ERS). In this method the sample is illuminated with 1.06um photons from a YAG laser with power intensities on the order of a KW/cm^2. The 1.06um photons simultaneously perform several functions. First the acceptors are neutralized by exciting the electrons from the acceptors to the deep EL2 donors. The neutral EL2 donors are then optically converted to the inactive, metastable state, leaving behind the neutral acceptors. Lastly, electronic Raman scattering from neutral acceptors can be observed Stokes-shifted from the laser energy by the difference between the ground and various excited states of the acceptors, predominanted by the 1s-2s splitting. This technique has been recently touted as a method of quantitative determination of acceptor concentration since it has an internal standard [85W] [86Wa] [85Ka]. The standard is due to the simultaneously observed Raman scattering from LO phonons whose intensity is a property of the bulk crystal independent of the impurity concentration. Thus, once a calibration has been established, the ratio of the intensity of the Raman scattering signal from the acceptors compared with the intensity of the LO phonon Raman signal will yield the absolute acceptor concentrations. As with the SPL techniques, different acceptors can be distinguished by their chemical shifts. While appealing due to its internal reference, Raman scattering is extremely weak and hence practical limits on detectable impurity concentration are much higher than for SPL.

Figure 4.7 shows a comparison of the SPL and ERS techniques. A

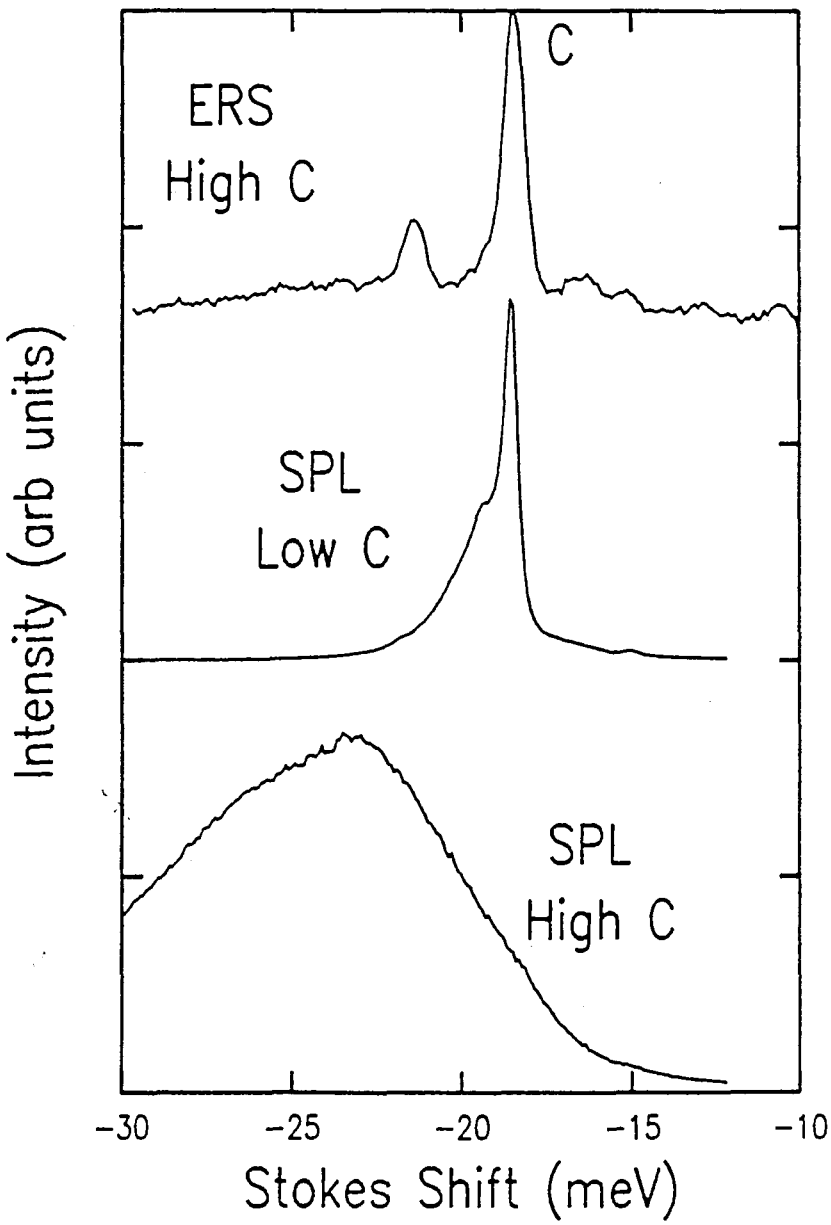

Fig. 4.7. Comparison of SPL and ERS on the same sample (top and bottom) containing large amounts of C ($3.3\times10^{16}cm^{-3}$) as well as SPL from a sample containing a low concentration of C (middle). ERS works best where SPL fails, but is not sensitive enough for the sample containing a small amount of C.

SPL spectrum of a sample with large carbon concentration ($3.3x10^{16}cm^{-3}$) is shown at bottom of the figure. At this concentration the SPL signal is severely smeared out (compared with the low carbon concentration at Fig 4.4) since donor-acceptor pairs are no longer isolated from the neighbors and consequently the SPL technique is no longer useful for resolving different acceptors. An ERS spectrum of the same sample is shown at the top of the Fig. 4.6. This spectrum, unlike the SPL spectrum, is narrow and contributions from C and Zn acceptors are clearly visible. Even at this concentration of carbon the ERS signal is extremely weak and collection of a spectrum takes one hour with a scanning spectrometer. The ERS peaks do not suffer the same broadening as compared to the SPL since only spatially much more compact neutral acceptors and not the neutral donors with very large and hence easily perturbed wavefunctions are involved.

4.5. Conclusion

Selective pair luminescence(SPL) is used to determine the relative concentrations of the shallow acceptors C, Zn, Si(Cd), Ge and Mg in semi-insulating GaAs. We present the data for Mg for the first time and investigated the dependence of the SPL spectra on the excitation energy, excitation intensity, temperature and impurity concentration in semi-insulating GaAs. The results show that SPL has the strongest signal with the excitation energy about 1509.5meV, the SPL technique is useful at low excitation intensity ($0.05mW/mm^2$), and the resolution of the SPL spectra is good below temperatures of 20K. The SPL spectra can quantitatively determine the relative concentration of the shallow acceptors from low (below $10^{14}cm^{-3}$) to high impurity concentration ($\sim 2\times10^{16}cm^{-3}$).

The SPL technique is a sensitive, non-destructive, fast and reliable technique. Since it is easy to separate the different acceptor lines by choosing the best excitation energy and since SPL works well at low excitation intensity and over a quite substantial ranges of impurity concentration and temperature, it can be used for routine characterization.

The ERS technique is not suitable for routine acceptor characterization of semi-insulating GaAs since the current semi-insulating GaAs has acceptor concentration of order $<1\times10^{15}cm^{-3}$. The two techniques are complementary since the ERS technique works best at high concentrations where SPL is useless, and SPL has the sensitivity to be useful at concentrations well below those currently achievable in present state-of-the-art growth.

CHAPTER 5 IDENTIFICATION OF THE DONORS

5.1. Introduction

The identification of shallow donors in semi-insulating GaAs is technologically important, since the identification and elimination of the sources of undesired impurity contamination during growth is considerably aided by a knowledge of the chemical nature of the impurities. However, in GaAs, discrimination of shallow donors is hampered by the very light electron effective mass ($m_e=0.07m_o$), resulting in very extended wavefunctions and consequently very small chemical shifts (<0.1meV). Even the two-electron satellite technique, which uses the full chemical shift, and is sometimes able to resolve different chemical impurities in epitaxially grown GaAs [77O] [88W], is unable to resolve different shallow donors in semi-insulating GaAs due to the larger linewidths. It is, fortunately, possible to resolve the chemical shifts of the donors in semi-insulating GaAs by applying a strong magnetic field to produce a large compression of the wave functions of the shallow donors [88H].

Besides the shallow donors, the well known deep donor is located at 750meV below conduction band in semi-insulating GaAs. It is usually referred to as the level EL2, since no clear identification of its physical and chemical origin has been done so far [88B]. This deep donor plays an important role in compensation mechanisms in undoped semi-insulating materials. It will be shown here that this level gives

rise to a specific absorption band in the near infrared [81M], the identification of which is achieved without any ambiguity. The optical absorption measurements enable us to measure the concentration of EL2, even in the thin device-thickness wafers (~1mm thick), without having to modify or destroy the sample.

5.2. Magneto-photoluminescence

The optical transitions used to identify the residual shallow donors resulted from the recombination of donor bound excitons. Specifically, the initial state of this transition is the n=1 state of the neutral donor bound exciton (D°,X) containing an unpaired hole. The final state is the donor in the N=2 excited state containing an unpaired electron. In semi-insulating GaAs, donors can be identified using resonant PL, but the addition of a large magnetic field is required.

The magnetic field serves two purposes [84D]: first it compresses the wavefunction perpendicular to the field, resulting in a greater electron amplitude in the central cell region and hence in a larger chemical shift; secondly, it separates components of different orbital angular momentum, reducing spectral interference. When (D°,X) recombine in a magnetic field, the excited 2s and 2p terminal states of the donor are separated. In addition, the field splits the 2p state into $2p_{-1}$, $2p_{0}$, and $2p_{+1}$ state. In GaAs, the total 1s to 2s (or 2p) zero field shift is about 5meV and the difference between donors is typical 0.05-0.30 meV at 10T [88H].

The magneto-photoluminescence experiments is carried out in a custom-built split-pair 7 T superconducting magnet cryostat in the Voigt geometry (**B** is normal to **K**). The optical throughput of f/6 is considerably reduced from that of the other dewars. In this particular cryostat, the sample chamber is completely separate from the magnet helium reservoir. For temperature at 4.2K and below, the sample

chamber is filled with liquid helium. For temperature above 10K, a crude but effective system is used whereby He gas is transferred into the sample chamber using a transfer siphon. To achieve the necessary spectral resolution, the 600-groove/mm gratings were replaced by 1200-groove/mm gratings.

Figure 5.1 shows three magneto-photoluminescence spectra. The bottom spectrum is from an MOCVD (metalorganic chemical vapor deposition) grown epitaxial sample in which the dominant donor is known to be Ge. Besides the strong Ge $2p_0$ two-electron replica, there are also some smaller peaks due to S and Si. In the middle is a spectrum from a semi-insulating GaAs sample that contains predominantly S and a small amount of Ge. The top sample also contains predominantly S without any detectable amount of Ge. It appears to contain an as yet unidentified donor labelled X, which has also previously been reported in semi-insulating GaAs [88H], but more recent results suggest that X may be a S-related transition from an excited BE initial state [90B]. Table 5.1 lists the energies of magneto-photoluminescence lines of shallow donors.

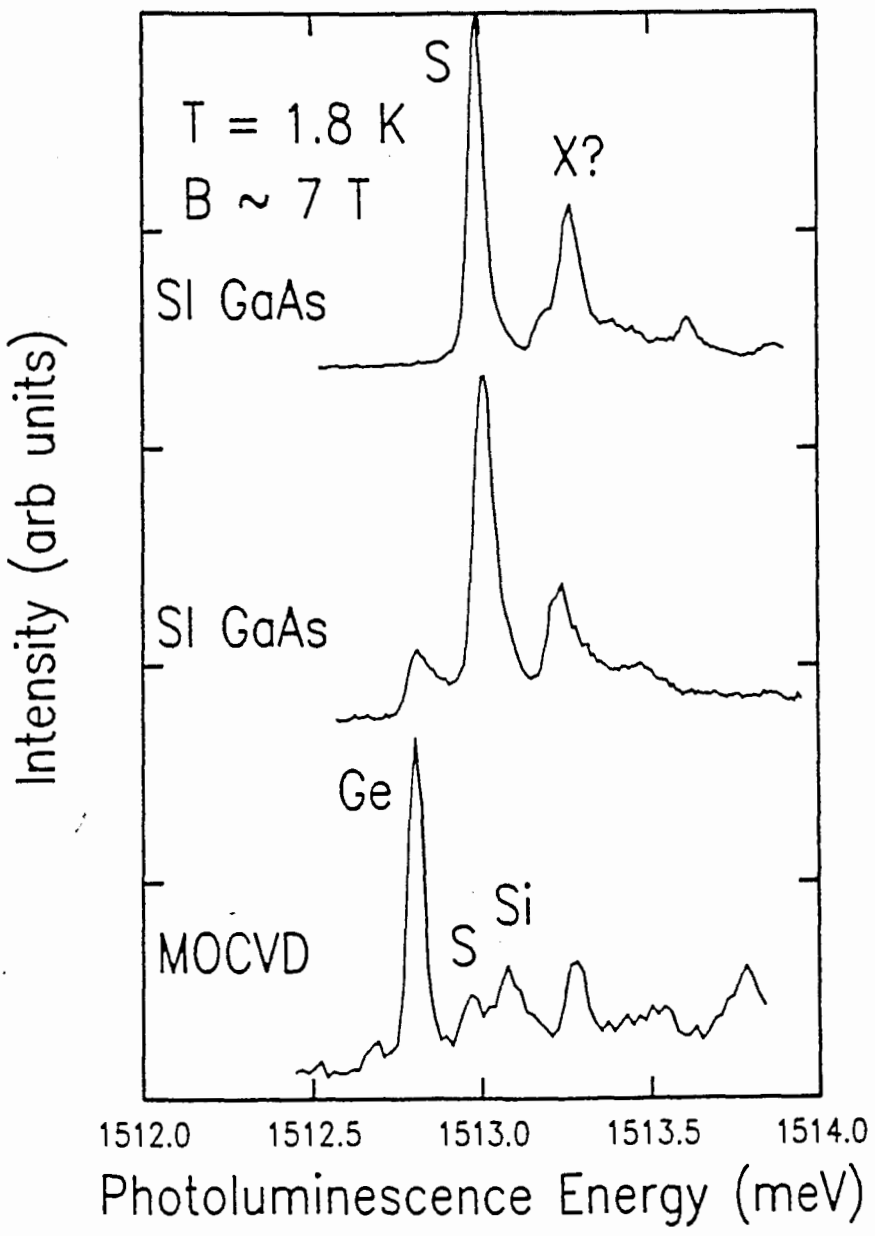

Fig. 5.1. Magneto-photoluminescence for shallow donor identification for two semi-insulating GaAs samples (above) and a MOCVD sample (bottom). The peaks are the $2p_0$ two-electron satellites of the donor bound excitons. The S.I. GaAs samples contain mostly S with sometimes Ge and as yet unidentified donor labelled X.

Table 5.1 Identification of shallow donors in GaAs (meV)

	MBE GaAs [82S]	MOCVD GaAs (±0.05)	S.I.GaAs (±0.05)
magnetic field	9.0T	7T	7T
splitting S--Si	0.12	0.08 S: 1513.05 Si: 1513.13	
splitting S--Se/Sn	0.09		
splitting S--Ge	-0.20	-0.18 S: 1513.05 Ge: 1512.87	-0.19 S: 1512.95 Ge: 1512.74
splitting S--X [88H]			0.23 S: 1512.95 X: 1513.18

5.3 Optical Absorption for Deep Donor EL2

The origin and nature of the EL2 center have been a subject of controversy since its first observation [88B]. Despite a great effort to understand EL2, there has been no clear explanation until now. Several models have been proposed to account for the nature of EL2. Most rely on the atomic displacement near the defect due to a transition between a normal and metastable state (i.e. an excited state for which all possible quantum transitions to lower state are forbidden at low temperature). The simplest models consists of an As_{Ga} antisite defect (i.e., an As atom occupying what is normally a Ga site) with vacancy [82M] [85B] or an interstitial [82V] [85B]. More complicated models such as an As_i (i.e., an As interstitial) with a divancacy [87W], families of EL2 levels [83T], and a complex center involving Ga_{As} antisite and C_{As} acceptor that leads to a strong lattice relaxation were proposed [87J] [88B].

The microscopic model proposed by von Bardeleben [87B] seems to account for much of what is known experimentally, but it is not without crucial problems. One key factor necessary for the validity of the model of von Bardeleben is the existence of an acceptor level associated with the normal state $EL2^0$ and a metastable state $EL2^*$. The normal state corresponds to an As_{Ga} antisite with an arsenic interstitial in the second-neighbor position and the metastable state corresponds to an As_{Ga} antisite with an As_i in the first-neighbor position.

Perhaps the most discussed and intriguing property of EL2 is its

photoquenching behavior, which has been observed in photocapacitance [79M] [81C] [82V], photoluminescence [82L] [84Y], photoconductivity [76L] [78P], and infrared absorption [81M] [89Ba] [900]. It is well known, for instance, that semi-insulating GaAs exhibits an absorption band in the 1000 to 1300meV range which has been attributed to the EL2 defect. This absorption is believed to be due to an intracenter transition between the EL2 ground state ($EL2^0$) at midgap and an excited state resonant with the conduction band. It can be completely quenched by irradiating the material with photons of about 1100 to 1200 meV energy. The photoquenching effect ($EL2^0$ to $EL2^*$) occurs when the defect is transformed from its normal state ($EL2^0$) to a metastable state ($EL2^*$). The structure of the metastable state $EL2^*$ is very little known. It is commonly assumed to arise from a large lattice relaxation and to lie in the band gap but no conclusive evidence can be cited to pinpoint the exact location of this level.

There is, however, some error in this absorption method due to other absorption mechanisms in this energy region and optical effects such as multiple internal reflections. The technique can be improved with a different measurement. First the absorption is measured; then without moving the sample, the EL2 is optically converted to its metastable state and the absorption measurement is repeated to get difference signal proportional only to the neutral EL2 concentration.

The EL2 absorption experiment was performed with the semi-insulating GaAs crystal which was cut to a size $3\times10\times25mm^3$ and then mechanically polished. The optical absorption measurements were performed along the largest dimension of the sample, which was

illuminated using white light filtered by a 3/4-m monochromator which was controlled by a IBM-PC computer. The light was closely focused on the front surface of the sample, which was held at 20K in a variable temperature cryostat. The transmitted light was detected with an intrinsic Ge detector (North Coast E0817L) using standard lock-in techniques. All runs were made after cooling the samples in the dark.

Figure 5.2 presents a spectacular effect of quenching of this optical absorption. The top curve is the no-phonon, intracenter absorption peak recorded at 20K after cooling the sample in the dark, which is subsequently optically bleached with a 3W ordinary flash light for 10 minutes. Complete quenching of absorption is observed in this case. After this bleaching process, the intracenter absorption is absent but can be brought back with a 10-minutes, 150K anneal as shown in bottom of figure 5.2.

Such a behavior can precisely be explained by the very peculiar property of the EL2 defect. the EL2 defect has a metastable state at low temperature. When it is in that metastable state, its electronic occupancy has been observed not to be changed by light. A strong lattice relaxation is thus believed to be associated with that metastable state. The complete quenching of absorption observed here can be directly related to the transfer of the level EL2 from its normal state $EL2^{0}$ to its metastable state $El2^{*}$ under the quenching light of high intensity.

For the actual determination of the neutral EL2 concentration, the measurement should be done at the peak of the photoionization curve at 1.0μm rather than at the position of the weak, non-phonon intracenter

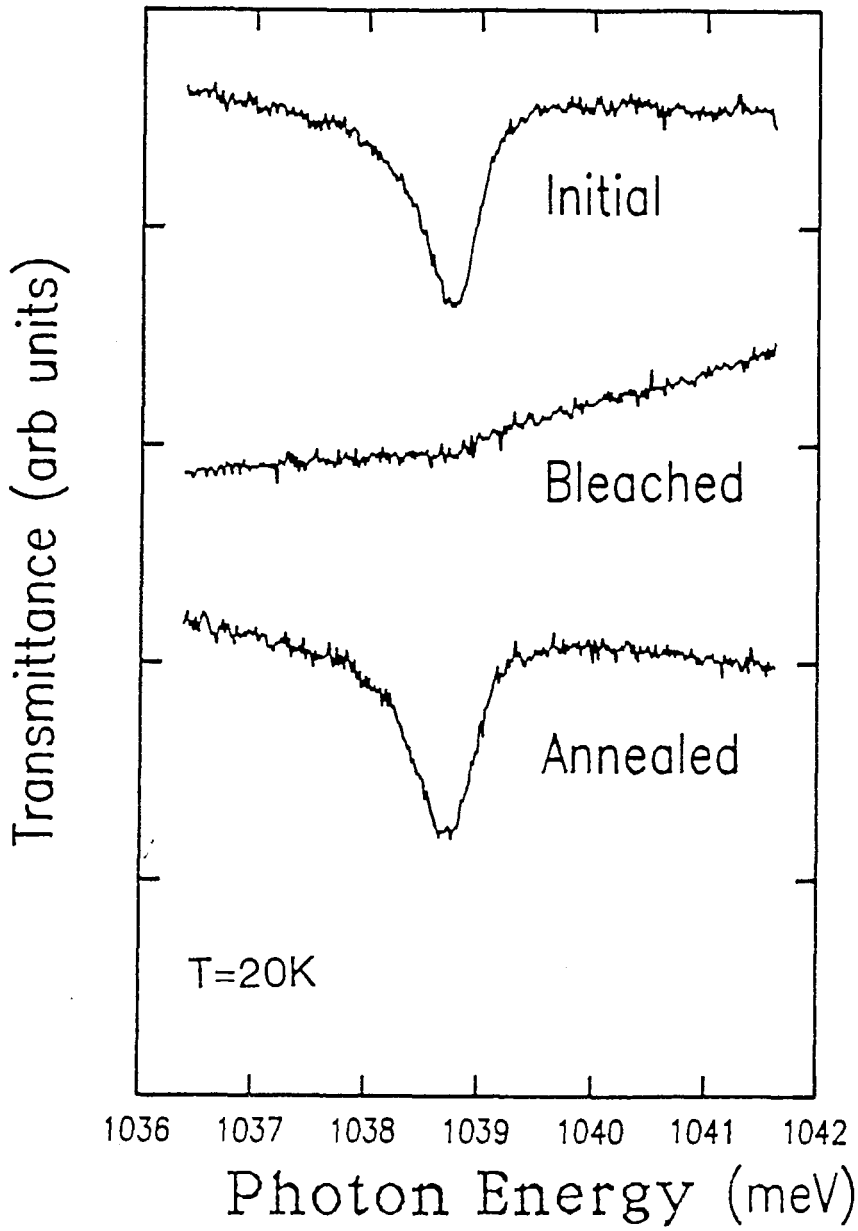

Fig. 5.2. EL2 optical absorption spectra at 20K from semi-insulating GaAs. The top spectrum shows the zero-phonon, intracenter absorption peak of EL2, middle spectrum was obtained after optical bleaching with ordinary flashlight, and the bottom spectrum was obtained after annealing at 150K for 10 minutes to recover the initial absorption.

absorption, but the principle is the same. The relation between EL2 concentration N_{EL2} and the near-infrared optical absorption coefficient data α due to photoionization of EL2 at 1.0μm at 4K is given by [900]:

$$N_{EL2} = 7.87\times10^{15}\ \alpha \qquad (cm^{-3}) \tag{5.1}$$

where the constant $7.87\times10^{15}cm^{-3}$ was experimentally determined by comparing the result of optical absorption with the photo-capacitance technique.

5.4. Conclusion

We have described the results concerning the high-field resonantly-excited magneto-photoluminescence for the identification of shallow donors in semi-insulating GaAs. The semi-insulating GaAs samples used in this study contain predominantly S, a small amount of Ge, and an unidentified donor labelled X.

The concentration of the neutral deep donor EL2, can be determined by measuring the near-infrared absorption due to the photoionization of EL2. The effects of other absorption mechanisms in the same energy region can be determined by first measuring an absorption spectrum, then bleaching the EL2 absorption by optically converting EL2 to its metastable state, and then repeating the absorption measurement. The change in absorption before and after bleaching is directly related to the original concentration of neutral EL2.

The story of the identification of EL2 is not yet over in particular because the character of the metastable state $EL2^{\bullet}$ is still not understood. Up to now all attempts to identify it experimentally have failed which suggests that the $EL2^{\bullet}$ has no associated gap state. Recently it has been proposed on theoretical grounds this state is an As split interstitial pair configuration [88B]. Apparently, this configuration fulfills all requirements necessary to explain the behavior and properties of the metastable state. However, a direct experimental verification is still lacking.

CHAPTER 6: QUANTITATIVE ASSESSMENT OF THE CARRIER DENSITY

6.1. Introduction

Optical characterization for semiconductors offers many advantages over electrical characterization, including its high sensitivity, simplicity, and non-destructive nature. However, it is difficult to obtain quantitative concentrations from optical measurements alone. Semi-insulating GaAs is a material whose desirable properties are obtained by compensation between a deep donor EL2 and shallow acceptors (in greater concentration than shallow donors). Both the presence of the deep donor and an excess of shallow acceptors are required for semi-insulating behavior.

In semi-insulating GaAs, quantitative knowledge of the donor and acceptor concentrations is very useful for predicting other properties, such as implant activation profiles, response to thermal annealing treatments, and elimination of undesired impurities.

In this chapter, we report, for the first time, that the concentrations of shallow acceptors, shallow donors, and the midgap donor EL2 may be quantitatively determined by all-optical methods. Using the compensation mechanism with the three level model in semi-insulating GaAs, we predict the room temperature carrier concentration, which is verified by the results of standard Hall effect measurements.

6.2. Compensation Mechanisms in Semi-insulating GaAs

The current model for the compensation mechanisms in semi-insulating GaAs is based on the interaction between the deep donor EL2 and the residual shallow acceptor and donor impurities. The concentrations of the acceptor impurities compensate, at least partially, the EL2 concentration so that the Fermi level lies in the vicinity of the EL2 midgap level.

We consider the three level model similar to one first proposed by Martin [80M] [83J] consisting of a deep donor level E_{EL2} and shallow donor and acceptor level E_D and E_A. For simplicity we shall assume that E_D is some average shallow donor energy, and similarly for E_A. We then denote the total shallow donor and acceptor concentrations as N_D and N_A, while N_{EL2} denotes the deep donor EL2 concentration.

The relevant equations consist of charge balance and suitable statistics. At room temperature the chemical potential ξ lies well within the gap, and the following exact and approximate formulas are valid:

$$p + N_D^+ + N_{EL2}^+ = n + N_A^- \tag{6.1}$$

$$n \cong N_C \exp[-(E_C - \xi)/kT] \tag{6.2a}$$

$$p \cong N_V \exp[-(\xi - E_V)/kT] \tag{6.2b}$$

$$N_A^- = N_A/\{1+\exp[(E_A - \xi)/kT]\} \cong N_A \tag{6.3a}$$

$$N_D^+ = N_D/\{1+\exp[(\xi - E_D)/kT]\} \cong N_D \tag{6.3b}$$

$$N_{EL2}^{+} = N_{EL2} /\{1+\exp[(\xi - E_{EL2})/kT]\} \qquad (6.3c)$$

where n/p = electron/hole concentrations; N_A^-/N_D^+, N_{EL2}^+ = ionized acceptor/donor concentrations; N_C/N_V = effective density of states (cm^{-3}) of conduction/valence bands; and E_C/E_V = conduction/valence band edges, with $E_g = E_c - E_v$ the gap energy.

Under the conditions stated previously, equations (6.2a) and (6.2b) imply that the electron and hole concentrations are governed by Boltzmann statistics, and equations (6.3a)-(6.3c) imply that all shallow donors and acceptors are ionized.

Since $(\xi - E_{EL2})$ may be comparable to kT, Equation (6.3c) can not be approximated, however, it is convenient to rewrite this equation in the form

$$N_{EL2}^{+} = N_{EL2}\left[\, 1 - \frac{1}{1 + \exp[(E_{EL2} - \xi)/kT]} \,\right]. \qquad (6.3d)$$

Two additional useful relations which may be obtained from equations (6.2a) and (6.2b), are

$$n_i^2 \equiv n\ p \cong N_C\ N_V \exp[-(E_C - E_V)/kT] \qquad (6.4)$$

$$\exp(-\xi/kT) = (N_C/n)\ \exp(-E_C/kT) \qquad (6.5)$$

Equation (6.4) yields the intrinsic carrier concentration n_i and equation (6.5) may be employed to eliminate the chemical potential ξ in

either equation (6.3c) or (6.3d).

By multiplying Equation (6.1) by n and using equations (6.2)-(6.5), one arrives at a cubic equation for the free electron density n in the three level model for semi-insulating GaAs:

$$n^3 + n^2[\, N_A - N_D + N_C \exp[(E_{EL2}-E_C)/kT]\,] + n\,[\, -n_i^2 + (N_A-N_D-N_{EL2})\, N_C \exp[(E_{EL2}-E_C)/kT]\,] - n_i^2\, N_C \exp[(E_{EL2}-E_C)/kT] = 0 \,. \qquad (6.6)$$

For undoped LEC semi-insulating GaAs, $n_i = 2.2\times10^6 cm^{-3}$ and $(N_A-N_D) \cong 10^{15} cm^{-3}$. The deep level is near the center of the gap $E_g/2$.

Finally, the parameter N_C is given by

$$N_C = 2\,(\, m_C^* KT/2\pi\hbar^2)^{3/2} \,, \qquad (6.7)$$

which for T=300K, evaluates to give $N_C = 4.3\times10^{17} cm^{-3}$. Similarly, for N_V which is needed in the calculation of n_i^2, we can write

$$N_V = (m_v^*/m_c^*)^{3/2} N_C = 10^{19}\ cm^{-3}.$$

For $(N_A - N_D) = 10^{15}\ cm^{-3}$, favorable conditions appear for stable near-intrinsic behavior since the carrier concentrations remain within an order of magnitude of the intrinsic carrier concentration even though N_{EL2} varies from 10^{15} to $10^{16} cm^{-3}$.

If $N_A > (\, N_D + N_{EL2})$ the material is p-type and the solutions for Eq. (6.6), using these parameters, can be approximated by

$$p \cong N_A - N_D - N_{EL2} \quad . \tag{6.8}$$

If $N_{EL2} > (N_A - N_D)$ the material is n-type, given by

$$n = [\, N_{EL2}/(N_A - N_D) - 1 \,](\, N_C/N_V)^{1/2} n_i \quad . \tag{6.9}$$

In general, for device purposes, one would prefer no deep traps such as Cu, Mn, Ga_{As}, and EL2 in semi-insulating GaAs. However, it would appear that the presence of some minimum number of deep traps rather close to midgap will always be required to produce semi-insulating GaAs substrates. In order to significantly reduce the concentrations of deep traps required, the concentration of shallow donors and acceptors will have to be reduced accordingly, requiring material of much higher chemical purity.

In the LEC semi-insulating GaAs provided by Johnson Matthey Electronics Ltd., the dominant shallow levels are acceptors, mostly due to C and Zn introduced in the growth process, which provide appropriate compensation for the shallow donors like S and Ge. EL2 then compensates for the excess of $N_A > N_D$. The deep acceptors including Cu, Mn, Ga_{As} are not usually seen in their production materials.

6.3. Quantitative Determination of the Shallow Acceptor Concentration

Using local vibration mode (LVM) absorption spectroscopy at 77K [86B], one can quantitatively assay the concentration of carbon, which is usually the dominant acceptor in semi-insulating GaAs. Carbon acceptors (C_{As}) exhibit a local vibration mode at 580 cm^{-1} (at 300K) [87Ba] [89Sa]. In this project, these measurements were performed by our co-operating company, Johnson Matthey Electronics.

The other acceptors do not have local vibrational mode signatures, but their concentration relative to the known carbon concentration can be quickly and accurately determined using selectively excited donor-acceptor pair luminescence as we described in the chapter 4. With excitation laser energy at 1510 meV, the relative concentration of Zn, Cd, and other shallow acceptors with respect to C are closely proportional to the relative intensities of their SPL lines, since pumping at 1510meV creates neutralized pairs at almost the same separation regardless of the species of shallow acceptors which are neutralized by creating holes in the excited state. We have experimentally verified that the peak intensity of the SPL features for C, Zn, Cd and Mg occurs at the excitation energy about 1510 meV in all samples as we discussed in chapter 4.

The top two spectra of Fig. 6.1 shows a comparison of the SPL spectra from the seed to tail end. Note the relative rise of the Zn concentration towards the tail, which clearly demonstrates the need to take acceptors other than carbon into account particularly in development boules grown for feed-stock evaluation.

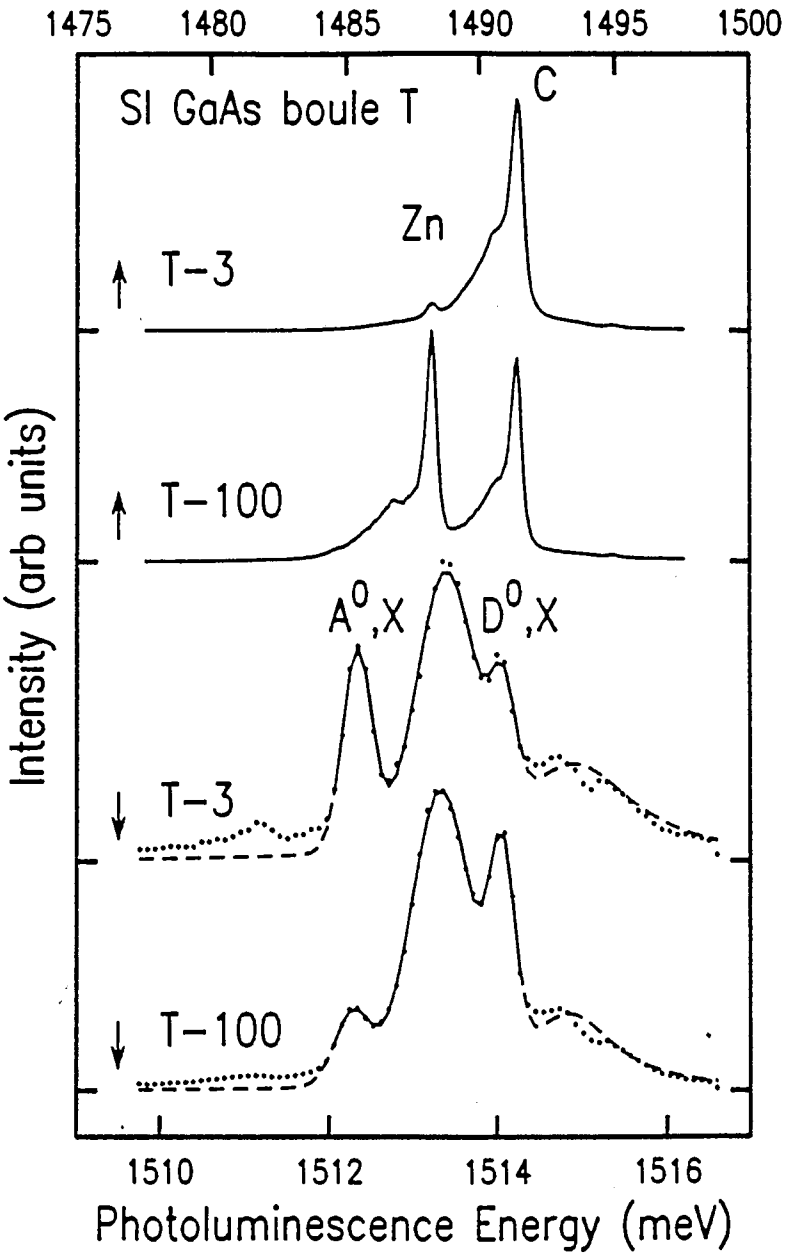

Fig.6.1. The top half of the figure shows SPL spectra of seed (T3) and tail (T100) samples with pumping at 1510meV, illustrating the relative rise of the Zn concentration toward the tail. At the bottom the line fitted to the resonant excitonic PL spectra of the same samples are shown. The solid line indicates the region over which the quality of the fit is evaluated while the dashed lines are the extension to the lower and higher energies. The lower two spectra (dots) are collected at 1.8K pumping with 500mW/cm^2 at 1518.1meV.

6.4. Quantitative Determination of the Donor Concentration

The determination of the concentration of the shallow donors N_D has been the stumbling block to a quantitative optical characterization of semi-insulating GaAs. The relative concentrations of various donors can be determined by the magneto-photoluminescence which has been described in the chapter 4, but not the total donor concentration.

We have found that resonant excitation at the n = 2 polariton energy (1518.1meV) produces a remarkable sharpening of the excitonic photoluminescence features in semi-insulating GaAs. A resonant spectrum is shown at the bottom of figure 6.2. This spectrum, unlike the ordinary photoluminescence spectrum excited at 2409meV (Ar-ion laser) shown at the top of figure 6.2, is narrow and the structures of the different excitons and polaritons are visible.

In order to solve the problems due to overlapping transitions of the polariton (X), neutral donor bound exciton (D^0,X), the combined free hole to neutral donor (D^0,h) and ionized donor bound exciton (D^+,X) line and the neutral acceptor bound exciton (A^0,X) shown at bottom of the figure 6.1, the quantitative contributions of these lines are analyzed. Figure 6.1 displays these resonant photoluminescence spectra obtained from seed and tail end samples of the test boule. The three lower energy lines are fitted using Gaussian lineshapes while a Lorentzian lineshapes is used for the polariton. The use of a Lorentzian lineshape for the polariton is admittedly not justifiable on physical grounds, but no suitable analytical expression is available. In any case, the purpose of fit to the polariton is merely to estimate

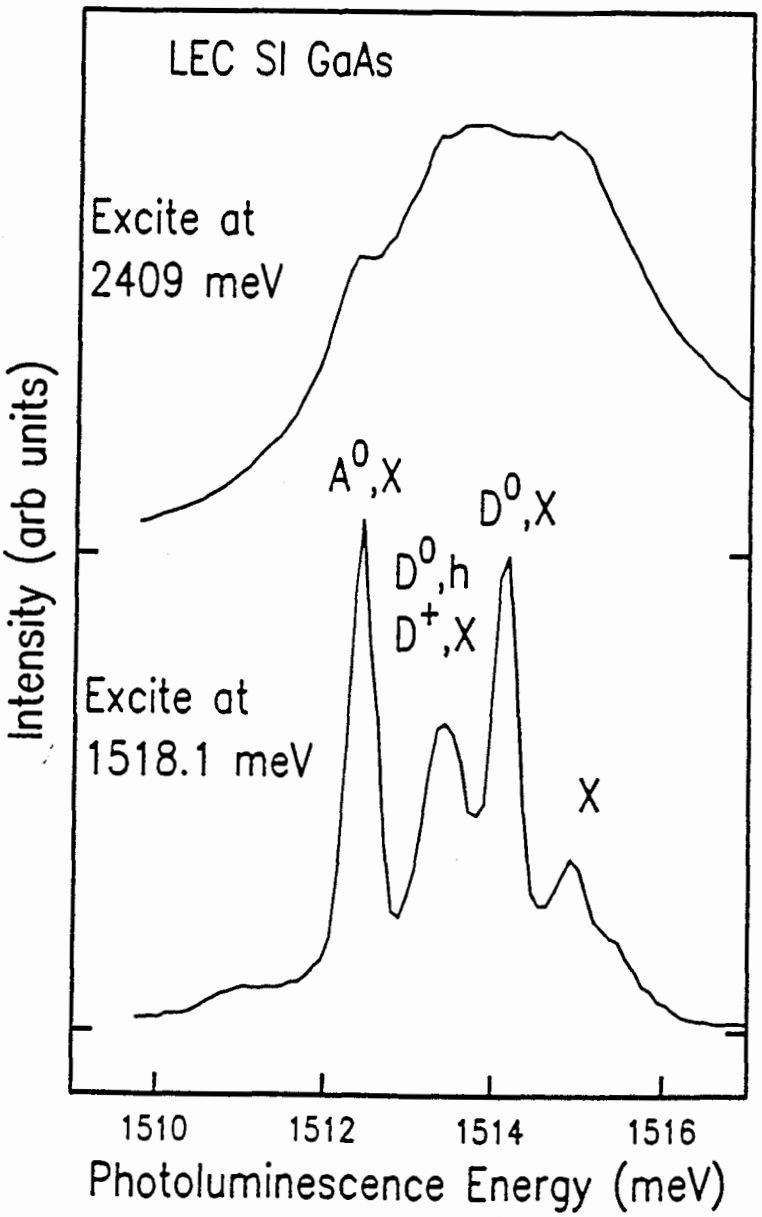

Fig. 6.2 comparison of PL spectra with far above-gap Ar-ion excitation (top) and a spectrum with resonant pumping of the n= 2 polariton at 1518meV. The Ar-ion excitation density is 15W/cm^2 while 500mW/cm^2 is used for the resonant spectrum.

the polariton contribution to the luminescence at lower energy. A description of the polariton lineshapes as a Lorentzian is adequate for this purpose. The shallow donor to acceptor ratio is then postulated to be proportional to the ratio of the integrated intensities of the (D^0,X) to (A^0,X) peaks (I_D to I_A). In order to determine N_D in terms of the Known N_A the only remaining unknown quantity is the proportionality constant k in

$$N_D = k\, N_A\, I_D/I_A \qquad (6.10)$$

The ratio k is determined experimentally from more than a hundred calibration samples as discussed below.

The EL2 concentration was determined from 4K infrared absorption spectroscopy as we mentioned in section 5.3, and are found to be 1.1×10^{16} cm^{-3} invariant over the length of the boule.

The Hall effect gives the concentration n(H) of free carriers. These measurements were performed by Johnson Matthey Electronics.

The equation (6.6) is solved for 140 samples using the optically determined values for kN_D, N_A and N_{EL2}. All quantities are known except the proportional constant k, which was allowed to vary in order to achieve the best fit with the electrically determined electron density n(H). This constant should be valid for all semi-insulating GaAs, and once determined, allows quantitative, non-destructive optical determination of N_D and thus n. Preliminary results indicate good agreement for samples where the three level model is valid. Figure 6.3 shows the results of the comparison of our optically determined n with

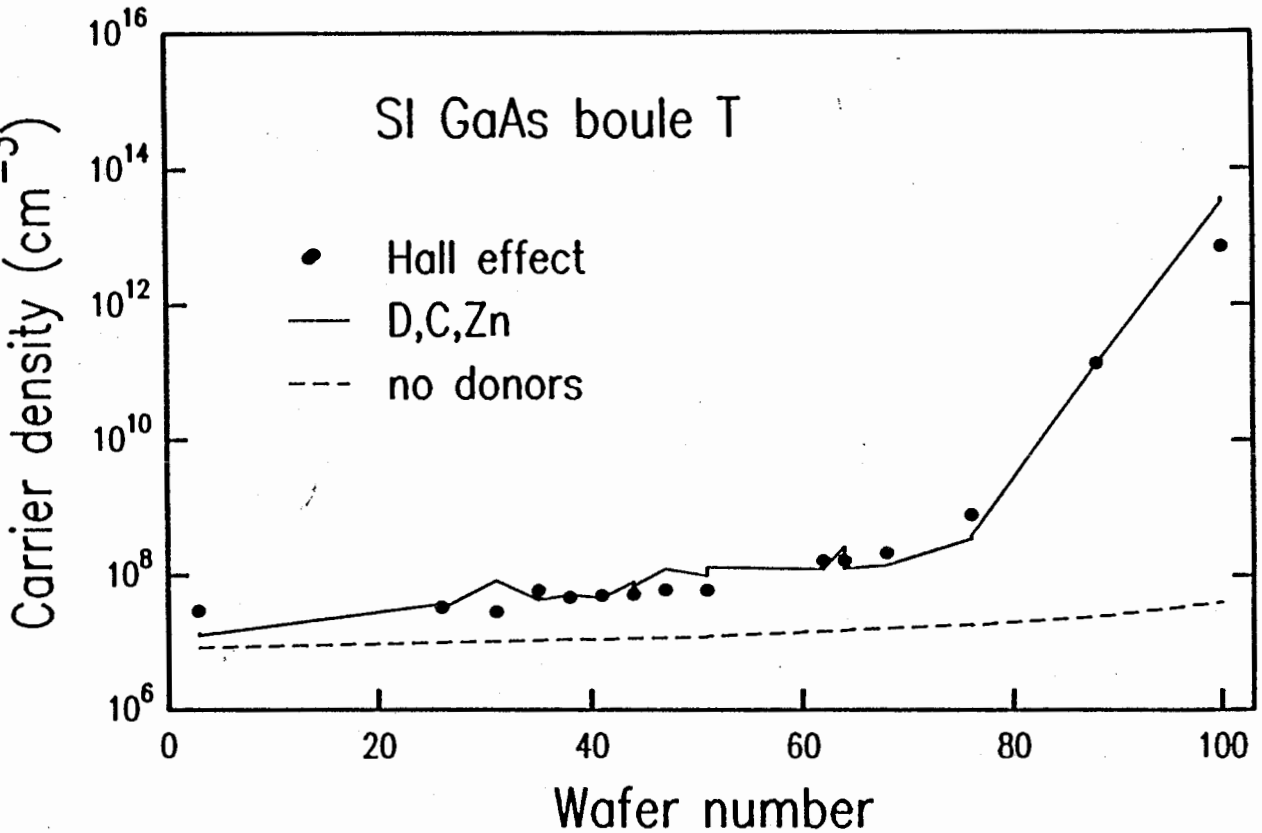

Fig. 6.3. Calibration of the optical determined carrier density (solid line) with the carrier density as determined by Hall effect measurements. The effect of neglecting the donor concentration is shown by the dashed line. The best fit is achieved with the single adjustable parameter for all sample set to k = 0.65.

n(H). The best fit is achieved with a value of 0.65 for the constant k, with an uncertainty of ± 0.1 due to the estimated uncertainty in determining the ratio I_A/I_D.

6.5. Conclusion

We have used a number of optical techniques for the concentration determination of shallow acceptors (N_A), shallow donors (N_D), and deep donor EL2 (N_{EL2}). For the acceptors, local vibrational mode absorption can determine the concentration of the carbon, while selective pair luminescence with excitation energy at 1510meV can determine the relative concentration of the other acceptors. For the shallow donors, resonant pumping of the first excited state of the polariton at 1518.1meV sharpened the photoluminescence spectrum sufficiently to allow a reliable measurement of the shallow donor to acceptor intensity ratio, which is proportional to the shallow donor and acceptor concentration ratio by a factor of 0.65. For the important deep donor EL2, absorption and bleaching experiments determine the neutral EL2 concentration.

We have demonstrated a quantitative, all optical technique for predicting the carrier density in semi-insulating GaAs. Using the parameters of N_A, N_D and N_{EL2}, the carrier density is calculated from the three level model.

The validity of the all optical technique was tested by comparing the predicted electron density to the measured Hall density. The results indicate a good agreement for the samples where the three level model is valid.

REFERENCES

51H Kun Huang. Proc. Roy. Soc. (London). **206**, 352(1951)

57P S. Pekar. Sov. Phys. JETP 6, 785(1957)

58H J.J. Hopfield. Phys. Rev. **112**, 1555(1958)

58T Y. Toyozawa. Prog. Theor. Phys. **20**, 50(1958)

60H J.R. Haynes. Phys. Rev. Lett. **4**, 361(1960)

62T Y. Toyozawa. Prog. Theor. Phys. **27**, 89(1962)

63C R.C. Casella. J. Appl. Phys. **44**, 1703(1963)

63H J.J. Hopfield, D.G. Thomas, and M. Gershenzon. Phys. Rev. Lett. **10**, 162(1963)

64H J.J. Hopfield in "Physics of Semiconductors" (Proc. 7th Int. Conf.), 725(1964)

65G D.G. Thomas, J.J. Hopfield, and W.M. Augustyniak. Phys. Rev. **140**, 202(1965)

65H C.H. Henry and J.J. Hopfield. Phys. Rev. Lett. **15**, 964(1965)

65T D.G. Thomas, J.J. Hopfield and W.M. Augustyniak. Phys. Rev. **140**, 202(1965)

66G M. Gershenzon in "Semiconductors and Semimetals". (edited by R.K. Willardson and A.C. Beer). Vol.2, Academic Press. 316(1966)

66R F.M. Ryan and R.C. Miller. Phys. Rev. **148**, 858(1966)

66S W.G. Spitzer in "Semiconductors and Semimetals" (edited by R.K. Willardson and A.C. Beer) Vol.3, Academic Press. 48(1966)

67L R.C.C. Leite and A.E. DiGiovanni. Phys. Rev. **153**, 841(1967)

67S R.R. Sharma and S. Rodriguez. Phys. Rev. **159**, 647(1967)

68B E.H. Bogardus and H.B. Bebb, Phys. Rev. **176**, 993(1968)

68L M.R. Lorentz, T.N. Morgan, G.D. Pettit, and W.J. Turner. Phys. Rev. **168**, 902(1968)

69D R. Dingle. Phys. Rev. **184**, 788(1969)

69L J.M. Lévy-Leblond. Phys. Rev. **178**, 1526(1969)

70L N.O. Lipari and A. Balderdash. Phys. Rev. Lett. **25**, 1660(1970)

71S G.E. Stillman, David M. Larsen, and C.M. Wolfe. Phys. Rev. Lett. 27(15), 989(1971)

72B H.B. Bebb and E.W. Williams in "Semiconductors and Semimetals" (edited by R.K. Willardson and A.C. Beer) Vol.**8**, Academic Press. 182(1966).

73D P.J. Dean. in "Luminescence of Crystals, Molecules and Solution" (edited by F. Williams), Plenum Press. 538(1973)

73S D.D. Sell, S.E. Stokowki, R. Dingle, and J.V. DiLorenzo. Phys. Rev. **B7**, 4568(1973)

75A D.J. Ashan, P.J. Dean, D.T.J. Hurle, B. Mullin, and A.M. White. J. Phys. Chem. Solids **36**, 1041(1975)

76L A.L. Lin, E. Omelianovski, and R.H. Bube. J. Appl. Phys. **47**,

1852(1976)

77O Masashi Ozeki, Kuninori Kitahara, Kenya Nakai, Akihiro Shibatomi, Koichi Dazai, Shinji Okawa, and Osamu Ryuzan. Jpn. J. Appl. Phys. 16(9), 1617(1977)

77W C. Weisbuch and R.G. Ulbrich. Phys. Rev. Lett. 39, 654(1977)

78P G.P. Peka, V.A. Brodovoi, I. I.Mishova, and L.Z. Mirets. Sov. Phys. Semicond. **12**, 540(1978)

78T Michio Tajima. Appl. Phys. Lett. **32**(11), 719(1978)

79A K. Aoki. Phys. Lett. **72A**, 63(1979)

79M A. Mitonneau and A. Mircea. Solid State Commun. **30**, 157(1979)

79Y P.Y. Yu and F. Evangelisti. Phys. Rev. Lett. **42**, 1642(1979)

80J M. Jaros. Adv. Phys. **29**, 409(1980)

80K P.B. Klein, P.E.R. Nordquist, and P.G. Siebermann. J. Appl. Phys. **51**, 4861(1980)

80M G. M. Martin, J.P. Farges, G. Jacob, J.P. Hallais and G. Poiblaud. J. Appl. Phys. **51**(5), 2840(1980)

81C A. Chantre, G. Vincent, and D. Bois. Phys. Rev. **B23**, 5335(1981)

81M G.M. Martin. Appl. Phys. Lett. **39**(9), 747(1981)

82B J.S. Blakemore. J. Appl. Phys. **53**(10), R123(1982)

82D P.J. Dean. Prog. Cryst. Growth, Chapter. 5, 89(1982)

82H D.E. Holmes and P.W. Yu. IEEE Trans. Electron Devices. **ED-28**, 1095(1982)

82Ha A.T. Hunter and T.C. McGill. Appl. Phys. Lett. **40**(2), 169(1982)

82K C. Korot and C.A. Stolte. IEEE Trans. Electron Devices. **ED-29**, 1059(1982)

82L P. Leyral, G. Vincent, A. Novailhat, and G. Guillot. Solid State Commun. **42**, 67(1982)

82M S. Makram-Ebeid, D. Gantard, P. Devillard, and G.M. Martin. Appl. Phys. Lett. **40**, 161(1982)

82R D.C. Reynolds, C.W. Litton, E.B. Smith, and K.K. Bajaj. Solid State Comm. **44**(1), 47(1982)

82Ra E.I. Rashba and M.D. Sturge. "Excitons", North-Holland Publishing Company, 14(1982)

82S G.E. Stillman, T.S. Low, T. Nakanisi, T. Udagawa, and C.M. Wolfe. Appl. Phys. Lett. **41**(2), 185(1982)

82V G. Vincent, D. Bois, and A. Chantre. J. Appl. Phys. **53**, 3643(1982)

83J E.J. Johnson, T.A. Kafalas, and R.W. Davies. J. Appl. Phys. **54**(1), 204(1983)

83K D.W. Kisker, H. Tews, and W. Rehm. J. Appl. Phys. **54**(3), 1322(1983)

83R D.C. Reynolds, K.K. Bajaj, C.W. Litton, and E.B. Smith. Phys. Rev. **B28**, 3300(1986)

83T M. Taniguchi and T. Ikoma. J. Appl. Phys. **54**, 6448(1983)

83N G.F. Neumarh and K. Kosai in "Semiconductors and Semimetals" (edited by R.K. Willardson and Albert C. Beer). Vol.19, Academic Press. 3(1983)

84D P.J. Dean, M.S. Skolnick, and L.L. Taylor. J. Appl. Phys. **55**(4), 957(1984)

84H S.R. Hetzler, T.C. McGill, and A.T. Hunter. Appl. Phys. Lett. **44**, 793(1984)

84R D.C. Reynolds, P.C. Colter, C.W. Litton, and E.B. Smith. J. Appl. Phys. **55**(6), 1610(1984)

84Y P.W. Yu. Appl. Phys. Lett. **44**, 330(1984)

85A F. Askary and Peter Y. Yu. Phys. Rev. **B31**, 6643(1985)

85B W. Bloss, E.S. Koteles, E.M. Brody, B.J. Sowell, J.P. Salerno, and J.V. Gormley. Solid State Comm. **54**, 103(1985)

85K E.S. Koteles, J. Lee, J.P. Salerno, and M.O. Vassell. Phys. Rev. Lett. **55**, 867(1985)

85Ka E.S. Koteles, S. Zemon, and P. Norris. Inst. Phys. Conf. ser. No.79 Chapter4, 259(1985)

85W K. Wan and R. Bray, Phys. Rev. **B32**, 5265(1985)

86B M.R. Brozel, E.J. Foulkes, R.W. Series and D.T.J. Hurle. Appl. Phys. Lett. **49**(6), 337(1986)

86P D. Paget and P.B. Klein. Phys. Rev. **B34**(2), 971(1986)

86S T. Steiner. Ph.D. Thesis, Simon Fraser University (1986)

86Sa B.J. Skromme, S.S. Bose, and G.E. Stillman. J. Electr. Matls. **15**(6), 345(1986)

86Sb T. Steiner, M.L.W. Thewalt, E.S. Koteles and J.P. Salerno. Phys. Rev. **B34**, 1006(1986)

86V J. van de Van and L.J. Giling. J. Appl. Phys. **60**(10), 3735(1986)

86W S.P. Watkins. Ph.D. Thesis, Simon Fraser University(1986)

86Wa J. Wagner, H. Seelewind, and V. Kaufmann. Appl. Phys. Lett. **48**(16), 1054(1986)

87B H.J. von Bardeleben, J.C. Bourgoin, D. Stievenard, and M. Lannoo. "GaAs and Related Compounds". 399(1987)

87Ba J.S. Blakemore. J. Appl. Phys. **62**, 4528(1987)

87C Shigefusa Chichibu, Santoru Matsumoto and Takeshi Obokata. J. Appl. Phys. **62**, 4316(1987)

87F L.A. Farrow, C.J. Sadroff and M.C. Tamargo. Appl. Phys. Lett. **51**(23), 1931(1987)

87J J. Jimenez, P. Hernandez, J.A. de Saja, and J. Bonnafe. Phys. Rev. **B35**, 3832(1987)

87W J.F. Wager and J.A. Van Vechten. Phys. Rev. **B35**, 2330(1987)

88B J.C. Bourgoin, H.J. von Bardeleben and D. Stievenard. J. Appl. Phys. **64**(9), R65(1988)

88C S. Charbonneau. Ph.D. Thesis, Simon Fraser University(1988)

88H T.D. Harris, M. S. Skolnick, and R. Bhat. Appl. Phys. Lett. **52**(2), 389(1988)

88I Takayuki Iino, Michio Tajima, and Koichi Ishida. J. Appl. Phys. **63**(11), 5454(1988)

88N S. Nilsson and L. Samuelson. Solid State Comm. **67**(1), 19(1988)

88S A.G. Steele. Ph.D. Thesis, Simon Fraser University(1988)

88W S.P. Watkins, G. Haacke, and H. Burkhard. Appl. Phys. Lett. **52**(5), 401(1988)

89B F. Bridges, G. Davies, J. Robertson, and A.M. Stoneham. J. Phys.: Condens. Matter **2**, 2875(1989)

89Ba J.S. Blakemore, L. Sargent, and R.S. Tang. Appl. Phys. Lett. **54**(21), 2106(1989)

89M M. Maciaszek, R.P. Bult, D.W. Rogers, T. Steiner, Yu Zhang, S. Charbonneau, and M.L.W. Thewalt. Can. J. Phys. **67**, 421(1989)

89Ma M.O. Manasreh, W.C. Mitchel, and D.W. Fisher. Appl. Phys. Lett. **55**(9), 864(1989)

89S T. Steiner, Yu Zhang, S. Charbonneau, A. Villemaire, M.L.W. Thewalt, M. Maciaszek and R. P. Bult. Can. J. Phys. **67**, 242(1989)

89Sa L. Sargent and J.S. Blakemore. Appl. Phys. Lett. **54**(11), 1031(1989)

89Z S. Zemon and G. Lambert. Solid State Comm. **70**(9), 855(1989)

90B D.J.S. Beckett. Ph.D. Thesis, Simon Fraser University(1990)

90O P. Omling and L. Samuelson. Presented at 6th Conf. on semi-insulating III-V Materials, May, 1990. Toronto

90S T.W. Steiner, Yu Zhang, M.L.W. Thewalt, M. Maciaszek and R.P. Bult. Presented at 6th Conf. on semi-insulating III-V Materials, May, 1990. Toronto

90Sa T.W. Steiner, Yu Zhang, M.L.W. Thewalt, M. Maciaszek and R.P. Bult. Appl. Phys Lett. **57**(7), 647(1990)